localization of tau (Fig. 1*A*,*B*, high magnification). The recognition of these neurons by MC-1 also reflects pathological changes in tau conformation as seen in human AD brains. These findings were specific to the hippocampus, as the striatum and cortex did not display CP13- or MC-1-positive neurons in any of the genotypes tested (supplemental Figure S2, available at www.jneurosci.org as supplemental material).

Western blotting of dissected hippocampus from 6-month-old mice revealed an increase in immunoreactivity for AT8, which recognizes phosphorylation of serine 202 and threonine 205, and PHF-1, which detects phosphorylated serine 396 and 404, in PS cDKO;WtTau animals (Fig. 1*C*). Similar experiments performed in dissected septum did not reveal differences between genotypes, most likely due to the small number of CP13- and MC-1-positive neurons in that area (data not shown). The AT8 results corroborate our findings that CP13 immunoreactivity, and therefore ser202 phosphorylation, is increased in the dentate gyrus of these mice. Increased PHF-1 site phosphorylation suggests a progression toward paired-helical filament development and represents the furthest degree of tau pathology detected in our studies. Consistent with this assessment, Campbell-Switzer silver stain did not reveal any neurofibrillary tangles in any of the genotypes at this age (data not shown), indicating that late-stage pathology is not yet present.

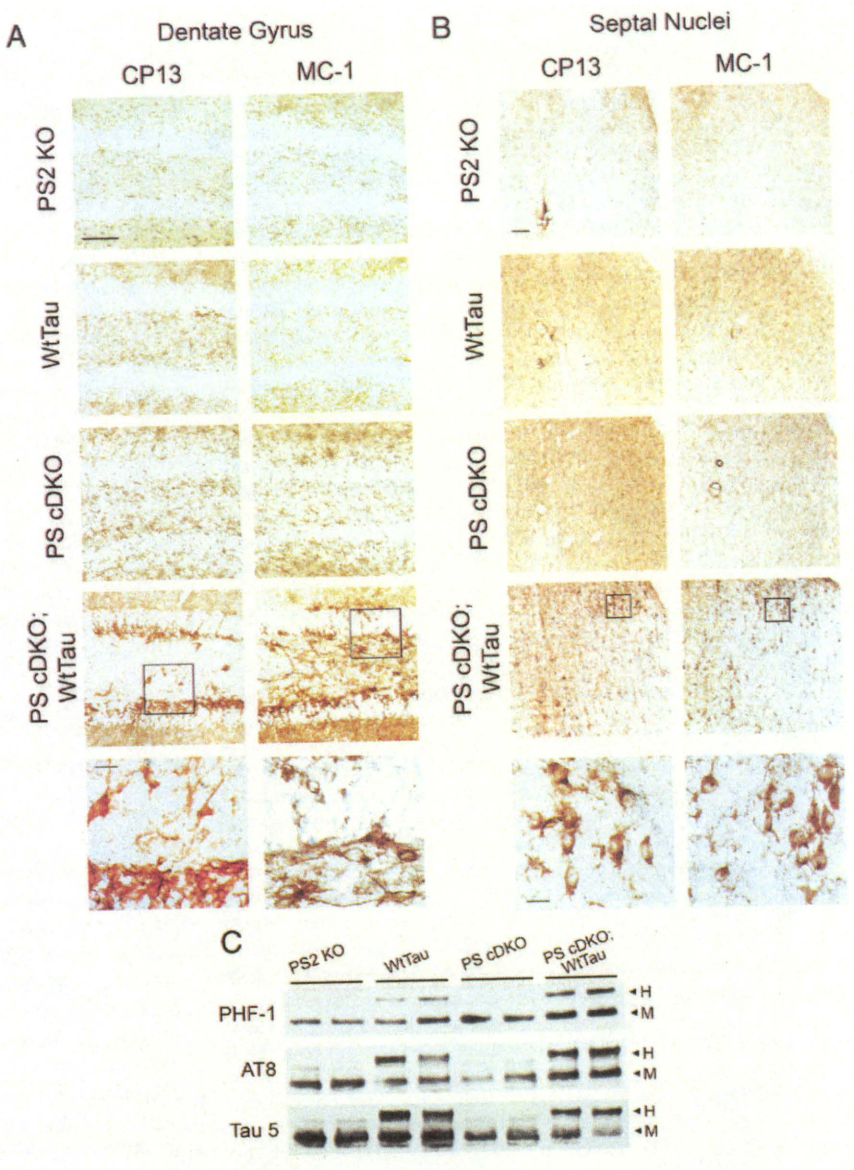

Figure 1. Tau pathology in 6-month-old PS cDKO;WtTau mice. ***A***, Representative images from the dentate gyrus showing CP13 (left) and MC-1 (right) immunostaining of PS2 KO, WtTau, PS cDKO, and PS cDKO;WtTau mice. ***B***, Representative images of CP13 and MC-1 immunostaining of a region including both the dorsolateral septal nucleus (upper right of each panel) and the medial septum (lower left of each panel). High-magnification insets show characteristic somatodendritic immunoreactivity in PS cDKO; WtTau neurons. Scale bars, 10 μm for inset images, 50 μm for all others. ***C***, Representative Western blots of phosphorylated (PHF-1 and AT8) and total (Tau 5) tau in hippocampal tissue homogenates dissected from 6-month-old mice show increased tau phosphorylation in PS cDKO;WtTau animals. H, human transgenic tau; M, mouse endogenous tau.

The expression of WtTau in PS cDKO mice leads to a reduction in anterograde axonal transport rates

Because tau hyperphosphorylation can impair axonal trafficking, we used Mn^{2+}-enhanced magnetic resonance imaging (MEMRI) to measure the efficiency of fast axonal transport. This method takes advantage of multiple useful features of manganese: 1) Mn^{2+} ions are paramagnetic and thus can serve as contrast agents for MRI; 2) as a calcium (Ca^{2+}) analog, Mn^{2+} exploits the cellular machinery responsible for uptake and vesicular packaging of Ca^{2+} to be effectively introduced to the neuron and its transport system; and 3) Mn^{2+} moves anterogradely along microtubules via fast axonal transport, allowing measurements of its synaptic accumulation to reflect overall transport rates (Mendonça-Dias et al., 1983; Burnett et al., 1984; Geraldes et al., 1986; Cory et al., 1987; Fornasiero et al., 1987; Sloot and Gramsbergen, 1994; Tindemans et al., 2003; Cross et al., 2008; Minoshima and Cross, 2008). We chose to measure trafficking in the olfactory system because it provides a convenient and pathologically relevant site for measurement of Mn^{2+} transport; ions can be administered noninvasively via nasal lavage and olfactory deficits have been well documented in patients with Alzheimer's disease (Mesholam et al., 1998; Peters et al., 2003).

Figure 2*A* shows representative images from 6-month-old PS2 KO and PS cDKO;WtTau mice at the first and last time points with outlined areas emphasizing signal enhancement. We tested PS2 KO, WtTau, PS cDKO, and PS cDKO;WtTau mice at 2 and 6 months of age and found that mice of all genotypes exhibited normal rates of transport at the younger age, indicating that the system is not developmentally impaired (Fig. 2*B*). At 6 months, however, PS cDKO;WtTau mice displayed a reduction ($\sim$50%, $p < 0.001$) in the rate of axonal transport compared with controls (Fig. 2*C*). This reduced rate was remarkably consistent between PS cDKO;WtTau animals (Fig. 2*D*). Interestingly, neither WtTau nor PS cDKO mice showed deficits at this age, providing evidence for a genetic interaction between presenilin and tau.

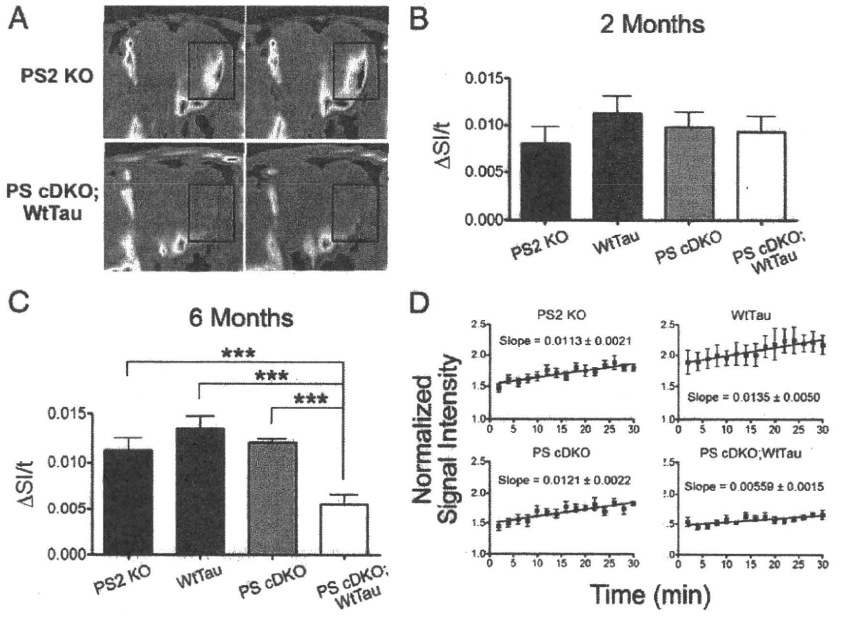

Figure 2. Age-dependent reduction in axonal transport rates of PS cDKO;WtTau mice. ***A***, Representative MEMRI color map images from PS2 KO controls and PS cDKO;WtTau mice at 6 months of age showing signal enhancement (emphasized by rectangular outline) between the first image (left) and the last image (right) of the series. ***B***, Axonal transport rates are normal in 2-month-old PS2 KO, WtTau, PS cDKO, and PS cDKO;WtTau mice. ***C***, Axonal transport rates at 6 months are selectively reduced in PS cDKO;WtTau mice. ***D***, Linear regression of all data points from each genotype of 6-month-old mice. Given slopes are graphically represented and statistically analyzed in ***C***). $\Delta SI/t$ = change in normalized signal intensity over time = rate of axonal transport. $^{***}p < 0.001$.

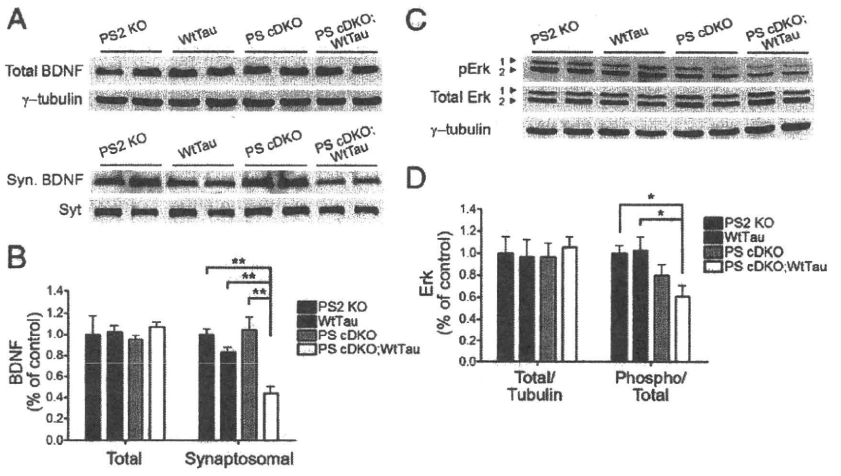

Figure 3. Decreased synaptosomal BDNF levels and Erk1/2 activation in the hippocampus of 6-month-old PS cDKO;WtTau animals. ***A***, Representative Western blots of total BDNF and BDNF from synaptosome fractions (BDNF). ***B***, Quantification of normalized BDNF band densities relative to control (PS2 KO). ***C***, Representative Western blots of total and phospho-Erk1/2. ***D***, Quantification of normalized Erk1/2 band densities relative to control. Loading controls were as follows: synaptotagmin (Syt) for synaptosomal BDNF and γ-tubulin for all others. $^{*}p < 0.05$, $^{**}p < 0.01$.

PS cDKO;WtTau mice exhibit reductions in synaptic brain-derived neurotrophic factor levels and Erk activation

To investigate the consequences of decreased axonal transport, we next examined brain-derived neurotrophic factor (BDNF) levels in the hippocampus. BDNF synthesis and anterograde trafficking occur within the hippocampus, but some hippocampal BDNF is also received anterogradely from the entorhinal cortex (Conner et al., 1997; Caleo and Cenni, 2004). BDNF is reduced in the brains of patients with AD, and recent work has shown that administration of BDNF into the entorhinal cortex can improve cell signaling, cognition, and neuronal survival in various mammalian models of AD through transport and signaling to the hippocampus (Murer et al., 2001; Gauthier et al., 2004; Nagahara et al., 2009). We therefore sought to determine whether the observed axonal transport deficit in PS cDKO;WtTau mice would cause a decrease in BDNF trafficking to the hippocampus, thus impairing its downstream signaling. Although total BDNF levels were unchanged in the hippocampi of PS2 KO, WtTau, PS cDKO, and PS cDKO;WtTau mice at 6 months of age, synaptosomal BDNF was decreased in PS cDKO;WtTau mice (Fig. 3*A*,*B*, $p < 0.01$), indicating a reduction in localization of BDNF to the synapse. Synaptotagmin undergoes anterograde transport through a mechanism distinct from that of BDNF and therefore served as both a loading control for the synaptosome fraction and a separate confirmation of the specific change in BDNF synaptic localization. The quality of synaptosomal fractionation was determined by Western blots for enrichment of the synaptic proteins PSD-95 and NMDA receptor 1 (supplemental Fig. S3, available at www.jneurosci.org as supplemental material).

BDNF binds to its receptor, Tropomycin-related kinase B (TrkB), at the synapse to initiate downstream signaling through three main pathways: the phosphatidylinositol 3-kinase (PI3K)-Akt pathway, the phospholipase Cγ1 (PCγ1)-Ca^{2+} pathway, and the Ras-mitogen-activated protein kinase (MAPK)-Erk1/2 pathway (Kaplan and Miller, 2000). Total levels of Erk were unchanged in all genotypes at 6 months of age, but activation of Erk through phosphorylation was specifically reduced in PS cDKO;WtTau mice (Fig. 3*C*,*D*, $p < 0.05$). Preliminary immunoblotting experiments did not detect changes in expression or activation of certain members of the PI3K or PCγ1 pathways (supplemental Fig. S4, available at www.jneurosci.org as supplemental material), but the possibility of altered signaling cannot be excluded. These data suggest that impaired transport of BDNF to the synapse leads to reduced downstream signaling through Erk.

Additional expression of WtTau worsens contextual memory deficits in PS cDKO mice at 6 months of age

Because of Erk's well established role in learning and memory, we used the conditioned fear paradigm to test associative memory in 6-month-old mice. Impairments in contextual memory have been reported in PS cDKO mice as early as 2 months of age, and cued learning deficits have also been observed in these animals at 12 months of age (Saura et al., 2004; Chen et al., 2008). The

percentage of time the mice spent frozen during the initial phase of training, before exposure to conditioned and unconditioned stimuli, was unchanged across genotypes, suggesting that baseline activity and anxiety levels were similar in all tested animals (Fig. 4*A*, Immediate). Consistent with previous studies, we observed a significant decrease (~40%, $p < 0.01$) in freezing of PS cDKO mice during the context test, reflecting a defect in hippocampus-dependent associative memory. Interestingly, PS cDKO;WtTau mice exhibited an even larger impairment in contextual memory (~65%, $p < 0.001$ vs control), which was significantly worse than that of PS cDKO animals (Fig. 4*A*, Context Test, $p < 0.05$ vs PS cDKO). We did not detect a difference in freezing of 6-month-old mice of any genotype during the cued test, indicating that amygdala-mediated learning pathways were functioning properly and that contextual memory deficits were likely due to hippocampus-specific defects (Fig. 4*A*, Cued Test).

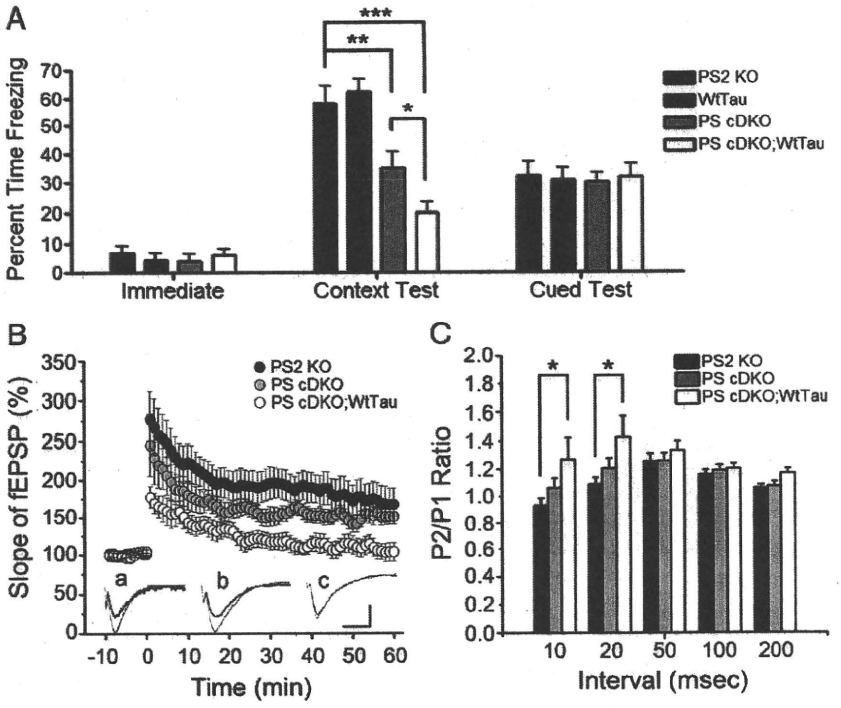

Figure 4. Hippocampal-dependent memory and synaptic plasticity impairments in PS cDKO;WtTau mice at 6 months of age. ***A***, Freezing behaviors during various phases of fear conditioning. Immediate freezing occurs during the initial exploratory period of training. Context test freezing represents the amount of time the mice froze during second exposure to the training chamber 24 h after training. Normalized cued test freezing is the difference between freezing during second exposure to the conditioned stimulus (CS) and freezing before CS in a novel chamber 24 h after training. ***B***, Following 10 min of baseline recording, theta burst stimulation (TBS) was delivered to the Schaffer collateral pathway. When compared with PS2 KO controls, PS cDKO;WtTau mice demonstrate significantly impaired LTP induction and maintenance at all time points tested; however, the difference between PS cDKO;WtTau and PS cDKO mice reaches significance only at the initial 3 and last 40 min. No significant difference is observed between PS cDKO and PS2 KO mice. Insets (***a–c***), Example fEPSP traces taken before and after TBS from PS2 KO, PS cDKO, and PS cDKO;WtTau mice, respectively (calibration, 1 mV, 5 ms). ***C***, Increased paired-pulse ratio in PS cDKO;WtTau mice at 10 and 20 ms interpulse intervals indicating altered presynaptic function in the hippocampus of PS cDKO;WtTau mice. $*p < 0.05$, $**p < 0.01$, $***p < 0.001$.

Presynaptic alteration underlies impaired Schaffer collateral LTP in PS cDKO;WtTau mice

In addition to being important modulators of learning and memory, BDNF and Erk play critical roles in LTP (Ying et al., 2002). We therefore examined field Schaffer collateral LTP in hippocampal brain slices of 6-month-old PS2 KO, PS cDKO and PS cDKO;WtTau mice. Potentiation induced by theta-burst stimulation (TBS) was significantly reduced and remained lower in PS cDKO;WtTau mice compared with PS2 KO controls ($p < 0.01$), but we found no significant differences between PS cDKO and PS2 KO animals (Fig. 4*B*). In contrast, the difference in LTP induction and maintenance between PS cDKO;WtTau and PS cDKO mice only reached significance during the first three and last 40 min ($p < 0.05$). To determine whether the deficit in LTP was related to presynaptic or postsynaptic defects, we conducted a paired-pulse protocol in which the ratio between the mean amplitudes of the second fEPSP over the first fEPSP (P2/P1 ratio) is inversely related to the initial release probability (Dobrunz and Stevens, 1997). In general, the smaller the probability of release to the first pulse, the more facilitated the response to the second pulse. We observed a significantly increased paired-pulse ratio in PS cDKO;WtTau mice compared with PS2 KO controls at the shortest interpulse intervals tested (Fig. 4*C*, $p < 0.05$), suggesting a reduced initial release probability in the PS cDKO;WtTau animals. Thus, altered presynaptic function may underlie the impaired Schaffer collateral LTP observed in PS cDKO;WtTau mice.

Expression of WtTau exacerbates cortical neurodegeneration in PS cDKO mice

PS cDKO mice are known to exhibit atrophy of the cerebral cortex by 6 months of age (Feng et al., 2004; Saura et al., 2004; Chen et al., 2008). Given our findings that the addition of WtTau can impair axonal transport, neurotrophin signaling, contextual memory, and LTP in PS cDKO mice, we hypothesized that these deficits could impact neuronal survival in this mouse model with proven susceptibility to cellular insults. We chose three-dimensional magnetic resonance imaging (3D MRI) to evaluate neurodegeneration because this method presents an opportunity to measure the volume of entire brain regions *in vivo*, eliminating the inconsistencies associated with histological processing. While our primary region of interest was the cerebral cortex, we also looked for the compensatory enlargement of ventricles that accompanies loss of cortical tissue. The volume of the cerebellum was analyzed as a negative control. Because no neuronal loss has been observed in WtTau mice up to 22 months of age, we elected to omit this group (Kimura et al., 2007). The other three genotypes were studied at 2 months of age to control for developmental differences in brain volumes and at 6 months to determine whether the aforementioned impairments at this age have an effect on neuron loss.

As expected, the volumes of all brain regions were comparable across genotypes at 2 months of age, demonstrating normal brain development in the absence of postnatal presenilin expression (Fig. 5*A*). As previously reported, PS cDKO mice exhibited a reduction in cortical volume at 6 months of age, which was accompanied by a compensatory increase in ventricular volume (Fig. 5*B*). Interestingly, PS cDKO;WtTau mice displayed even greater cortical atrophy at this age, supporting a role for tau in

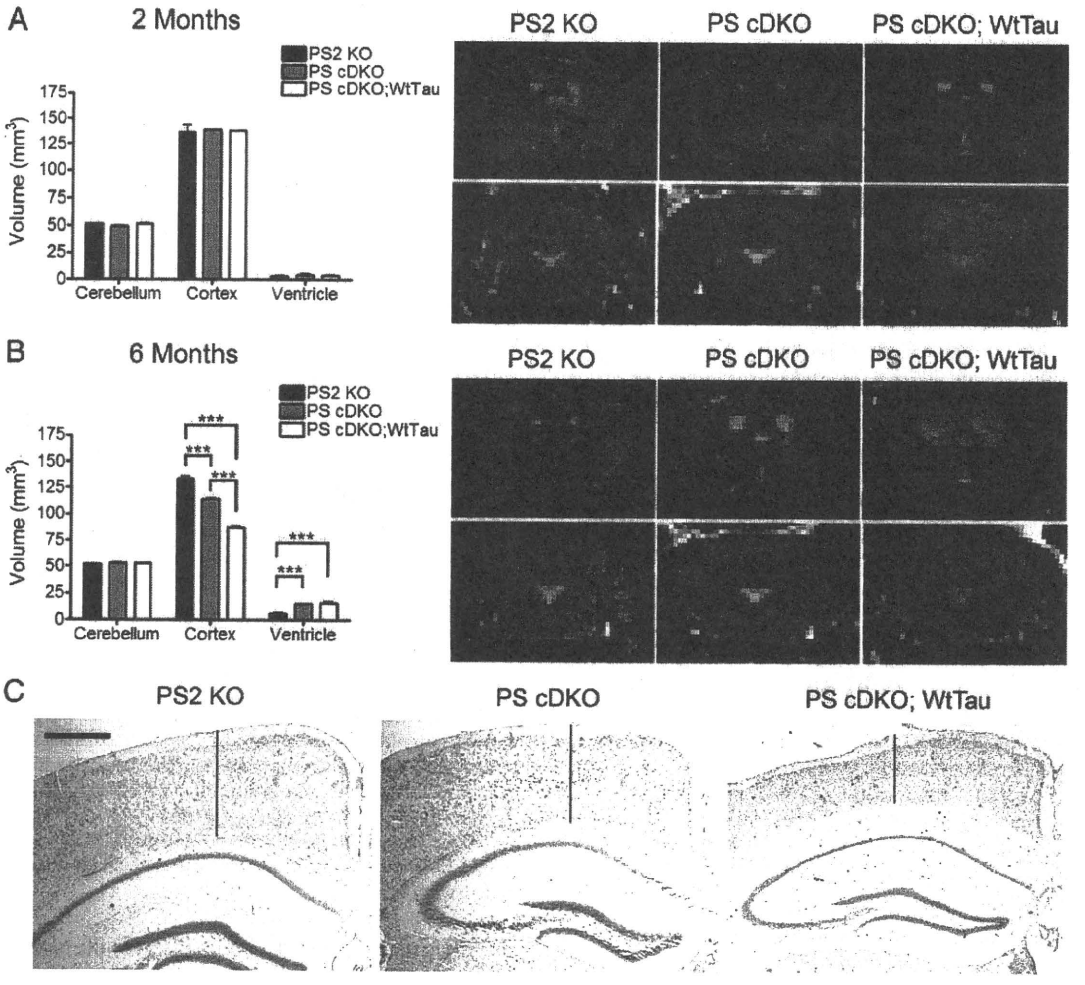

Figure 5. Increased cortical neurodegeneration in PS cDKO;WtTau compared with PS cDKO mice. ***A***, Volumes of cerebellum, cerebral cortex, and ventricles are normal in 2-month-old PS2 KO, PS cDKO, and PS cDKO;WtTau mice. Quantification of volumes (left) and representative 3D MRI images (right) show no obvious differences in structures between genotypes. ***B***, Cerebral cortical atrophy of PS cDKO mice is exacerbated in PS cDKO;WtTau animals at 6 months. Quantification of volumes (left) and representative 3D MRI images (right) show a decrease in cortical volume with compensatory increase in ventricular volume (top) in PS cDKO mice and, to a further degree, in PS cDKO;WtTau mice. No change in cerebellar volumes was detected (bottom). ***C***, Representative images from cresyl violet (Nissl)-stained frozen brain sections demonstrate cortical atrophy in 6-month-old PS cDKO and PS cDKO;WtTau mice as quantified in panel 5B. Vertical lines are provided to assist with visual assessment of cortical thickness at sites that are comparable between sections. Scale bar, 500 μm, $^{***}p < 0.001$.

this neurodegenerative phenotype (Fig. 5*B*, *C*). At both ages, cerebellar volumes remained stable across genotypes, indicating that changes in cortical and ventricular volumes resulted specifically from the CaMKIIα-regulated genetic modifications in PS cDKO and PS cDKO;WtTau mice.

Discussion

Although a large body of evidence supports some level of interaction between presenilin and tau in AD pathogenesis, the precise contributions of each have yet to be fully ascertained. Specifically, the role of wild-type human tau has been largely passed over in favor of study of mutant tau-expressing mouse models, which more readily develop tau pathology but do not accurately reflect the genetics of tau in AD. Here we have shown that expression of WtTau in PS cDKO mice can impair multiple cellular functions that are significant to the development of AD (Fig. 6). In these mice, tau hyperphosphorylation and pathological conformation were detected as early as 6 months of age in neurons of the septal nuclei of the basal forebrain and the dentate gyrus of the hippocampus. We determined that anterograde axonal transport was impaired specifically in PS cDKO;WtTau mice at this time point, suggesting a role for tau hyperphosphorylation and/or aggregation in this deficit. In the hippocampus, reduced synaptosomal BDNF in the context of normal levels of total BDNF provided additional support for the hypothesis that axonal transport is impaired in areas with tau pathology. The finding that Erk activation was also diminished in the hippocampus of PS cDKO;WtTau mice implied that this level of synaptic BDNF reduction was sufficient to decrease its downstream signaling. Deficient BDNF/Erk signaling had important consequences for contextual learning and memory, and long-term potentiation as well, as impairments in both were observed to a greater degree in PS cDKO mice expressing WtTau. Finally, the combination of these deficits led to an increase in cortical atrophy in PS cDKO;WtTau mice when compared with PS cDKO mice, suggesting that multiple mechanisms underlie the neurodegeneration in these mice, and possibly in AD.

The presence of tau pathology in the septal nuclei and dentate gyrus of PS cDKO;WtTau mice could have several implications for neuronal function in the hippocampus. Septal neurons are

known to project to the dentate gyrus in addition to other hippocampal and extrahippocampal regions. Lesion of septal cholinergic neurons or pharmacological inhibition of septohippocampal cholinergic signaling impairs hippocampal-dependent learning and memory, a deficit that can be rescued by administration of acetylcholine to the hippocampus (for review, see Parent and Baxter, 2004). This corresponds with the loss of cholinergic neurons in AD, which results in memory impairment that can be partially allayed by treatment with acetylcholinesterase inhibitors (Kása et al., 1997; Seltzer, 2006). In addition, pharmacological inhibition of cholinergic signaling by scopolamine has been shown to reduce protein levels of BDNF in the rodent hippocampus (Kotani et al., 2006). Although we did not detect a change in total levels of BDNF in the hippocampus, tau phosphorylation of a subset of neurons in the septohippocampal pathway would perturb the system to a significantlys lesser degree than global inhibition of cholinergic signaling. This limited tau phosphorylation also explains our inability to detect with Western blots the tau pathology observed with immunohistochemistry. Ultimately, the finding that interruption of cholinergic signaling can lead to reductions in downstream BDNF levels provides support for our model that disruption of septohippocampal signaling through tau hyperphosphorylation leads to reduced synaptic BDNF in the hippocampus. Furthermore, strong involvement of this pathway in hippocampal-dependent learning and memory implies a potential mechanism for the specific contextual memory deficit we observed in PS cDKO;WtTau mice.

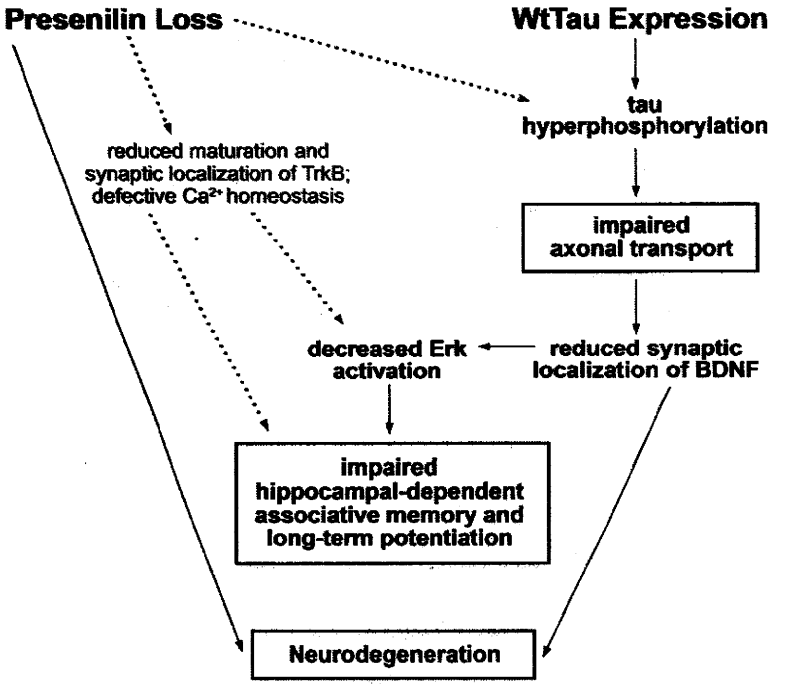

Figure 6. Model of neuronal dysfunction and neurodegeneration in PS cDKO;WtTau mice. Presenilin loss has been shown previously to increase tau phosphorylation, reduce TrkB receptor maturation and synaptic localization, and result in defective Ca^{2+} homeostasis (dotted lines; see Discussion for references). In combination with presenilin loss, expression of WtTau accelerates tau hyperphosphorylation, leading to impaired anterograde axonal transport of synaptic proteins such as BDNF. This decrease in BDNF at the synapse reduces downstream signaling, which, along with loss of presenilin, can directly affect neuronal survival. In addition, specific reduction of Erk phosphorylation/activation impairs hippocampal-dependent memory and long-term potentiation, phenotypes to which presenilin loss likely contributes through mechanisms outside the scope of this study. Boxed results were obtained from *in vivo* studies, with the exception of LTP.

The development of tau pathology and impaired axonal transport in PS cDKO;WtTau mice are likely mediated by changes in the activity of tau kinases. Levels of p25, a potent activator of the tau kinase Cdk5, have been shown to increase in PS cDKO mice by 9 months of age (Saura et al., 2004). Interestingly, loss of presenilin has also been shown to increase GSK3β kinase activity, leading to GSK3β-mediated phosphorylation of the motor protein kinesin to promote its release from its membrane-bound cargoes during anterograde axonal transport (Morfini et al., 2002; Pigino et al., 2003). GSK3β misregulation due to presenilin loss could also lead to tau phosphorylation, suggesting two possible mechanisms for kinase-mediated axonal transport defects in PS cDKO mice: directly through kinesin phosphorylation, and/or indirectly through tau phosphorylation. Because PS cDKO mice did not demonstrate impairment of axonal transport in our studies, tau phosphorylation appears to exert a more profound effect on trafficking than kinesin phosphorylation. Other kinases that phosphorylate tau could also be involved, and it is possible that a combination of small increases in multiple kinases, rather than large increases in a single kinase's activity, could be responsible for the tau phenotypes observed in our study.

While most neurotrophins undergo primarily retrograde axonal transport from the synapse to the cell body, anterograde transport of BDNF is seen in multiple pathways within the brain, including septal and cortical projections to the hippocampus and intrahippocampal circuits (for review, see Schindowski et al., 2008). Along with our observation that synaptic localization of BDNF is reduced, this supports the hypothesis that the defects in axonal transport detected in the olfactory system of PS cDKO; WtTau mice might extend to other brain regions, notably the hippocampus. Decreased Erk signaling in the hippocampus and functional deficits in hippocampal-dependent memory and synaptic plasticity in PS cDKO;WtTau animals further support this notion. In addition to a role for impaired axonal transport in reduced BDNF/Erk signaling, presenilin loss may contribute to this phenotype through other mechanisms. Loss of presenilin in primary neurons results in decreased maturation and membrane localization of TrkB, the primary receptor for BDNF (Naruse et al., 1998). This reduction in mature TrkB at the synaptic membrane could exacerbate an Erk signaling impairment caused by reduced synaptic BDNF. Although PS cDKO mice did not exhibit a statistically significant reduction in Erk activation, a downward trend was observed in these mice, supporting the existence of more than one mechanism underlying this phenotype. In fact, this could be the case with each of the phenotypes exhibited by PS cDKO mice that were exacerbated in PS cDKO;WtTau animals (i.e., contextual memory deficits and neurodegeneration).

Although LTP defects were not clearly demonstrated in PS cDKO mice, a trend toward reduced potentiation did exist. As with Erk signaling, other effects of presenilin loss could be contributing to this phenotype. LTP and other measures of synaptic plasticity require Ca^{2+} signaling, which is regulated by presenilin and is defective in familial AD mutants or PS-deficient mice (for

review, see Mattson, 2010). A recent study genetically and pharmacologically dissected the role of presenilin in Schaffer collateral neurotransmitter release and found that presynaptic loss of presenilin impairs theta-burst-induced LTP through impairment of calcium release (Zhang et al., 2009). This corresponds with our observation that in addition to LTP, paired-pulse facilitation is altered in PS cDKO;WtTau mice, indicating a presynaptic defect. Although these alterations in Ca^{2+} release could also affect Mn^{2+}, our administration of saturating doses of $MnCl_2$ and the lack of axonal transport impairment in PS cDKO mice make it unlikely that such a phenomenon occurred in our study. Our inability to detect LTP deficits in PS cDKO mice could be explained by differences in experimental setup or variation in mouse strains and transgenes between our study and previous reports. Because of the trend toward a decrease in PS cDKO vs PS2 KO mice in our present study, however, it is possible that a statistically significant difference would be observed with an increased sample size or a modified stimulation protocol.

Together, our data support a combined role for presenilin and tau in AD pathogenesis. Substantial evidence supports the notion that familial AD mutations in presenilin genes primarily result in PS loss of function, particularly with regard to γ-secretase cleavage of Notch, cadherins, and APP (Chen et al., 2002; Moehlmann et al., 2002; Wiley et al., 2005). In PS mutants, the cleavage of APP generates β-amyloid species in a ratio that favors the pathogenic Aβ42 over Aβ40, but this could result from decreased production of Aβ40, not excess Aβ42 (for review, see De Strooper, 2007). Presenilin mutations can also impair γ-secretase-independent functions, leading to defects in Wnt signaling and Ca^{2+} homeostasis (for review, see Shen and Kelleher, 2007). This evidence supports the use of PS cDKO mice to study the roles of presenilin and tau in AD pathogenesis. We have established that loss of presenilin alone results in a phenotype that can be enhanced and even expanded by the presence of wild-type human tau, leading to impairment of axonal trafficking, neurotrophin signaling, learning and memory, and synaptic plasticity, all of which culminate in neurodegeneration. These findings provide evidence for the convergence of multiple pathways in the progression of AD and indicate that subtle differences in protein composition (i.e., human vs mouse tau) can dramatically affect cellular processes governing neuronal function and survival.

References

Akins MR, Greer CA (2006) Cytoskeletal organization of the developing mouse olfactory nerve layer. J Comp Neurol 494:358–367.

Burnett KR, Goldstein EJ, Wolf GL, Sen S, Mamourian AC (1984) The oral administration of MnCl2: a potential alternative to IV injection for tissue contrast enhancement in magnetic resonance imaging. Magn Reson Imaging 2:307–314.

Caleo M, Cenni MC (2004) Anterograde transport of neurotrophic factors: possible therapeutic implications. Mol Neurobiol 29:179–196.

Chen F, Gu Y, Hasegawa H, Ruan X, Arawaka S, Fraser P, Westaway D, Mount H, St George-Hyslop P (2002) Presenilin 1 mutations activate gamma 42-secretase but reciprocally inhibit epsilon-secretase cleavage of amyloid precursor protein (APP) and S3-cleavage of notch. J Biol Chem 277:36521–36526.

Chen Q, Nakajima A, Choi SH, Xiong X, Tang YP (2008) Loss of presenilin function causes Alzheimer's disease-like neurodegeneration in the mouse. J Neurosci Res 86:1615–1625.

Conner JM, Lauterborn JC, Yan Q, Gall CM, Varon S (1997) Distribution of brain-derived neurotrophic factor (BDNF) protein and mRNA in the normal adult rat CNS: evidence for anterograde axonal transport. J Neurosci 17:2295–2313.

Cory DA, Schwartzentruber DJ, Mock BH (1987) Ingested manganese chloride as a contrast agent for magnetic resonance imaging. Magn Reson Imaging 5:65–70.

Cross DJ, Flexman JA, Anzai Y, Maravilla KR, Minoshima S (2008) Age-related decrease in axonal transport measured by MR imaging in vivo. Neuroimage 39:915–926.

De Strooper B (2007) Loss-of-function presenilin mutations in Alzheimer disease. Talking Point on the role of presenilin mutations in Alzheimer disease. EMBO Rep 8:141–146.

Dobrunz LE, Stevens CF (1997) Heterogeneity of release probability, facilitation, and depletion at central synapses. Neuron 18:995–1008.

Donoviel DB, Hadjantonakis AK, Ikeda M, Zheng H, Hyslop PS, Bernstein A (1999) Mice lacking both presenilin genes exhibit early embryonic patterning defects. Genes Dev 13:2801–2810.

Feng R, Rampon C, Tang YP, Shrom D, Jin J, Kyin M, Sopher B, Miller MW, Ware CB, Martin GM, Kim SH, Langdon RB, Sisodia SS, Tsien JZ (2001) Deficient neurogenesis in forebrain-specific presenilin-1 knockout mice is associated with reduced clearance of hippocampal memory traces. Neuron 32:911–926.

Feng R, Wang H, Wang J, Shrom D, Zeng X, Tsien JZ (2004) Forebrain degeneration and ventricle enlargement caused by double knockout of Alzheimer's presenilin-1 and presenilin-2. Proc Natl Acad Sci U S A 101:8162–8167.

Fornasiero D, Bellen JC, Baker RJ, Chatterton BE (1987) Paramagnetic complexes of manganese(II), iron(III), and gadolinium(III) as contrast agents for magnetic resonance imaging. The influence of stability constants on the biodistribution of radioactive aminopolycarboxylate complexes. Invest Radiol 22:322–327.

Gauthier LR, Charrin BC, Borrell-Pagès M, Dompierre JP, Rangone H, Cordelières FP, De Mey J, MacDonald ME, Lessmann V, Humbert S, Saudou F (2004) Huntingtin controls neurotrophic support and survival of neurons by enhancing BDNF vesicular transport along microtubules. Cell 118:127–138.

Geraldes CF, Sherry AD, Brown RD 3rd, Koenig SH (1986) Magnetic field dependence of solvent proton relaxation rates induced by Gd3+ and Mn^{2+} complexes of various polyaza macrocyclic ligands: implications for NMR imaging. Magn Reson Med 3:242–250.

Higuchi M, Lee VM, Trojanowski JQ (2002) Tau and axonopathy in neurodegenerative disorders. Neuromolecular Med 2:131–150.

Ittner LM, Fath T, Ke YD, Bi M, van Eersel J, Li KM, Gunning P, Götz J (2008) Parkinsonism and impaired axonal transport in a mouse model of frontotemporal dementia. Proc Natl Acad Sci U S A 105:15997–16002.

Kaplan DR, Miller FD (2000) Neurotrophin signal transduction in the nervous system. Curr Opin Neurobiol 10:381–391.

Kása P, Rakonczay Z, Gulya K (1997) The cholinergic system in Alzheimer's disease. Prog Neurobiol 52:511–535.

Kimura T, Yamashita S, Fukuda T, Park JM, Murayama M, Mizoroki T, Yoshiike Y, Sahara N, Takashima A (2007) Hyperphosphorylated tau in parahippocampal cortex impairs place learning in aged mice expressing wild-type human tau. EMBO J 26:5143–5152.

Kotani S, Yamauchi T, Teramoto T, Ogura H (2006) Pharmacological evidence of cholinergic involvement in adult hippocampal neurogenesis in rats. Neuroscience 142:505–514.

LaPointe NE, Morfini G, Pigino G, Gaisina IN, Kozikowski AP, Binder LI, Brady ST (2009) The amino terminus of tau inhibits kinesin-dependent axonal transport: implications for filament toxicity. J Neurosci Res 87:440–451.

Lazarov O, Morfini GA, Pigino G, Gadadhar A, Chen X, Robinson J, Ho H, Brady ST, Sisodia SS (2007) Impairments in fast axonal transport and motor neuron deficits in transgenic mice expressing familial Alzheimer's disease-linked mutant presenilin 1. J Neurosci 27:7011–7020.

Mattson MP (2010) ER calcium and Alzheimer's disease: in a state of flux. Sci Signal 3:pe10.

Mendonça-Dias MH, Gaggelli E, Lauterbur PC (1983) Paramagnetic contrast agents in nuclear magnetic resonance medical imaging. Semin Nucl Med 13:364–376.

Mesholam RI, Moberg PJ, Mahr RN, Doty RL (1998) Olfaction in neurodegenerative disease: a meta-analysis of olfactory functioning in Alzheimer's and Parkinson's diseases. Arch Neurol 55:84–90.

Mi K, Johnson GV (2006) The role of tau phosphorylation in the pathogenesis of Alzheimer's disease. Curr Alzheimer Res 3:449–463.

Minoshima S, Cross D (2008) In vivo imaging of axonal transport using MRI: aging and Alzheimer's disease. Eur J Nucl Med Mol Imaging 35 [Suppl 1]:S89–S92.

Moehlmann T, Winkler E, Xia X, Edbauer D, Murrell J, Capell A, Kaether C,

Zheng H, Ghetti B, Haass C, Steiner H (2002) Presenilin-1 mutations of leucine 166 equally affect the generation of the Notch and APP intracellular domains independent of their effect on Abeta 42 production. Proc Natl Acad Sci U S A 99:8025–8030.

Morfini G, Szebenyi G, Elluru R, Ratner N, Brady ST (2002) Glycogen synthase kinase 3 phosphorylates kinesin light chains and negatively regulates kinesin-based motility. EMBO J 21:281–293.

Murer MG, Yan Q, Raisman-Vozari R (2001) Brain-derived neurotrophic factor in the control human brain, and in Alzheimer's disease and Parkinson's disease. Prog Neurobiol 63:71–124.

Nagahara AH, Merrill DA, Coppola G, Tsukada S, Schroeder BE, Shaked GM, Wang L, Blesch A, Kim A, Conner JM, Rockenstein E, Chao MV, Koo EH, Geschwind D, Masliah E, Chiba AA, Tuszynski MH (2009) Neuroprotective effects of brain-derived neurotrophic factor in rodent and primate models of Alzheimer's disease. Nat Med 15:331–337.

Naruse S, Thinakaran G, Luo JJ, Kusiak JW, Tomita T, Iwatsubo T, Qian X, Ginty DD, Price DL, Borchelt DR, Wong PC, Sisodia SS (1998) Effects of PS1 deficiency on membrane protein trafficking in neurons. Neuron 21:1213–1221.

Parent MB, Baxter MG (2004) Septohippocampal acetylcholine: involved in but not necessary for learning and memory? Learn Mem 11:9–20.

Parks AL, Curtis D (2007) Presenilin diversifies its portfolio. Trends Genet 23:140–150.

Peters JM, Hummel T, Kratzsch T, Lötsch J, Skarke C, Frölich L (2003) Olfactory function in mild cognitive impairment and Alzheimer's disease: an investigation using psychophysical and electrophysiological techniques. Am J Psychiatry 160:1995–2002.

Pigino G, Morfini G, Pelsman A, Mattson MP, Brady ST, Busciglio J (2003) Alzheimer's presenilin 1 mutations impair kinesin-based axonal transport. J Neurosci 23:4499–4508.

Redwine JM, Kosofsky B, Jacobs RE, Games D, Reilly JF, Morrison JH, Young WG, Bloom FE (2003) Dentate gyrus volume is reduced before onset of plaque formation in PDAPP mice: a magnetic resonance microscopy and stereologic analysis. Proc Natl Acad Sci U S A 100:1381–1386.

Saura CA, Choi SY, Beglopoulos V, Malkani S, Zhang D, Shankaranarayana Rao BS, Chattarji S, Kelleher RJ 3rd, Kandel ER, Duff K, Kirkwood A, Shen J (2004) Loss of presenilin function causes impairments of memory and synaptic plasticity followed by age-dependent neurodegeneration. Neuron 42:23–36.

Schindowski K, Belarbi K, Buée L (2008) Neurotrophic factors in Alzheimer's disease: role of axonal transport. Genes Brain Behav 7 [Suppl 1]:43–56.

Seltzer B (2006) Cholinesterase inhibitors in the clinical management of Alzheimer's disease: importance of early and persistent treatment. J Int Med Res 34:339–347.

Shen J, Kelleher RJ 3rd (2007) The presenilin hypothesis of Alzheimer's disease: evidence for a loss-of-function pathogenic mechanism. Proc Natl Acad Sci U S A 104:403–409.

Sloot WN, Gramsbergen JB (1994) Axonal transport of manganese and its relevance to selective neurotoxicity in the rat basal ganglia. Brain Res 657:124–132.

Smith KD, Kallhoff V, Zheng H, Pautler RG (2007) In vivo axonal transport rates decrease in a mouse model of Alzheimer's disease. Neuroimage 35:1401–1408.

Spencer CM, Serysheva E, Yuva-Paylor LA, Oostra BA, Nelson DL, Paylor R (2006) Exaggerated behavioral phenotypes in Fmr1/Fxr2 double knockout mice reveal a functional genetic interaction between Fragile X-related proteins. Hum Mol Genet 15:1984–1994.

Tindemans I, Verhoye M, Balthazart J, Van Der Linden A (2003) In vivo dynamic ME-MRI reveals differential functional responses of RA- and area X-projecting neurons in the HVC of canaries exposed to conspecific song. Eur J Neurosci 18:3352–3360.

Tsien JZ, Chen DF, Gerber D, Tom C, Mercer EH, Anderson DJ, Mayford M, Kandel ER, Tonegawa S (1996) Subregion- and cell type-restricted gene knockout in mouse brain [see comments]. Cell 87:1317–1326.

Wiley JC, Hudson M, Kanning KC, Schecterson LC, Bothwell M (2005) Familial Alzheimer's disease mutations inhibit gamma-secretase-mediated liberation of beta-amyloid precursor protein carboxy-terminal fragment. J Neurochem 94:1189–1201.

Ying SW, Futter M, Rosenblum K, Webber MJ, Hunt SP, Bliss TV, Bramham CR (2002) Brain-derived neurotrophic factor induces long-term potentiation in intact adult hippocampus: requirement for ERK activation coupled to CREB and upregulation of Arc synthesis. J Neurosci 22:1532–1540.

Zhang B, Higuchi M, Yoshiyama Y, Ishihara T, Forman MS, Martinez D, Joyce S, Trojanowski JQ, Lee VM (2004) Retarded axonal transport of R406W mutant tau in transgenic mice with a neurodegenerative tauopathy. J Neurosci 24:4657–4667.

Zhang C, Wu B, Beglopolous V, Wines-Samuelson M, Zhang D, Dragatsis I, Sudhof TC, Shen J (2009) Presenilins are essential for regulating neurotransmitter release. Nature 460:632–636.

FEBS Letters 584 (2010) 3227–3232

FEBS Letters

journal homepage: www.FEBSLetters.org

Microtubule destruction induces tau liberation and its subsequent phosphorylation

Tomohiro Miyasaka [a,b,*], Sinji Sato [a], Yoshitaka Tatebayashi [a], Akihiko Takashima [a]

[a] Laboratory for Alzheimer's Disease, Brain Science Institute, The Institute of Physical and Chemical Research (RIKEN), 2-1 Hirosawa, Wako-shi, Saitama 351-0198, Japan
[b] Department of Neuropathology, Faculty of Life and Medical Sciences, Doshisha University, 1-3 Tatara Miyakodani, Kyotanabe-shi, Kyoto 610-0394, Japan

ARTICLE INFO

Article history:
Received 13 May 2010
Revised 9 June 2010
Accepted 10 June 2010
Available online 17 June 2010

Edited by Jesus Avila

Keywords:
Tau
Microtubule
Phosphorylation
Stathmin
Neurofibrillary tangle
Alzheimer's disease

ABSTRACT

Neurofibrillary tangle-bearing neurons, a pathological hallmark of Alzheimer's disease, are mostly devoid of normal microtubule (MT) structure and instead have paired helical filaments that are composed of abnormal hyperphosphorylated tau. However, a causal relationship between tau phosphorylation and MT disruption has not been clarified. To examine whether MT disruption induces tau phosphorylation, stathmin, an MT-disrupting protein, was co-expressed with tau in COS-7 cells. Stathmin expression induced apparent MT catastrophe and tau hyperphosphorylation at Thr-181, Ser-202, Thr-205, and Thr-231 sites. In contrast, c-Jun N-terminal kinase activation, or phosphatase inhibition, led to significant tau phosphorylation without affecting MT structure. These findings suggest that MT disruption induces subsequent tau phosphorylation.

1. Introduction

Tubulin heterodimers, α- and β-tubulin, assemble into microtubules (MTs), which are in a dynamic equilibrium with the non-polymerized form. Filamentous structures provide intracellular cytoskeleton in various cells and are especially enriched in neurons [1–4]. The extent of MT assembly is regulated by many factors such as temperature, protein-modification of tubulin, small molecules like taxol, and some MT-interacting proteins [5–7]. Because MTs have significant roles in a broad range of biological functions, including shaping the neuronal structure and transporting intracellular cargoes, it is reasonable to speculate that MT disruption, if any, profoundly affects neuronal architecture and function [8–11].

Tau proteins were identified as a factor promoting MT assembly and stabilization. MT assemblies are thought to be negatively regulated by tau phosphorylation [12,13]. To date, more than 40 serine (Ser) and threonine (Thr) residues have been identified as possible phosphorylation sites on tau [14]. Although the biological significance of individual phosphorylation sites is not known, it has been known that phosphorylation of Ser-262 (numbered according to the 441-residue tau) has a profound effect on its interaction with MTs [15].

Neurofibrillary tangles (NFTs) are a major neuropathological hallmark in brains affected by Alzheimer's disease (AD) and related diseases. The central nervous system diseases in which NFT formation is predominant are categorized as tauopathies. Because the areas in the brain that form NFTs often exhibit neuronal loss, the formation of these filamentous structures is assumed to be the crucial event in neuronal degeneration [16]. Abnormally phosphorylated tau is a major component of NFTs [17–19], which raises a possible link between phospho-tau accumulation and neurodegeneration and has led us to investigate their causal relationship. NFT-bearing neurons often accompany loss of MTs and tubulin [20–22]. This inverse relation can be observed across various animal models for tauopathy [23,24]. It remains unclear why MTs or tubulin are lost in the affected neurons. MT loss has also been found even in non-NFT-bearing neurons in the AD brain [22], suggesting that MT loss may precede tau phosphorylation and accumulation in brains affected by tauopathy. Therefore, we aimed to elucidate the possible link between MT loss and phospho-tau accumulation. The effects of drug-inducing MT depolymerization on expressed tau have been studied [25], which showed that the tau was dephosphorylated at specific sites. However, the impacts of cell-intrinsic MT-disrupter on tau phosphorylation have never been

Abbreviations: NFT, neurofibrillary tangle; AD, Alzheimer's disease; MT, microtubule; GSK3β, glycogen synthase kinase 3 beta; JNK, c-Jun N-terminal kinase; MEKK, mitogen-activated protein kinase/extracellular signal-regulated kinase kinase kinase; DMEM, Dulbecco's modified eagle's medium; FBS, fetal bovine serum; MOI, multiplicities of infection

* Corresponding author at: Department of Neuropathology, Faculty of Life and Medical Sciences, Doshisha University, 1-3 Tatara Miyakodani, Kyotanabe-shi, Kyoto 610-0394, Japan. Fax: +81 774 65 6135.
E-mail address: tomiyasa@mail.doshisha.ac.jp (T. Miyasaka).

0014-5793/$36.00
doi:10.1016/j.febslet.2010.06.014

addressed. Stathmin is a factor acting on MT disruption and/or a tubulin sequestration and is ubiquitously expressed in many cell types, including neurons [26,27]. Furthermore, SCG10, a neuron-specific homolog of stathmin, is known to increase in the brains of AD patients [28]. To study whether physiological MT disruption affects tau phosphorylation, tau and stathmin were co-expressed in COS-7 cells using adenovirus-mediated transfection.

2. Materials and methods

2.1. Materials

Anti-stathmin antisera against N- and C-terminal positions, STN1 (ASSDIQVKELEKRA) and STC1 (RKNKESKDPADETEAD) were raised against synthetic peptides conjugated with KLH. The anti-tau antibodies used were tau-c, which reacts with pan-tau [29]; AT270, AT8, and AT180, which react with phospho-Thr181, phospho-Ser202 and -Thr205, and phospho-Thr231 and -Ser235, respectively (Innogenetics, Gent, Belgium); PHF-1, which reacts with phospho-Ser396 and -Ser404 (a generous gift from P. Davies) [30]; and PS422 (BioSource International, Camarillo, CA). Anti-α-tubulin (DM1A) and anti-acetylated-α-tubulin (6-11B1) were purchased from Sigma (St. Louis, MO). Okadaic acid was purchased from Roche Diagnostics (Basel, Switzerland).

2.2. DNA constructs and expression in COS cells

Generation of recombinant adenovirus was performed as previously described [29]. Briefly, stathmin cDNA encoding amino acids 1–145 was amplified and inserted between the HindIII and XbaI sites of the pFLAG-CMV2 vector. The FLAG tagged-stathmin open reading frame was inserted into the pAxCAwt vector (Takara) at the SwaI site (designated pAxCA-F-stathmin) and the resulting cosmid was used to generate recombinant adenoviruses (designated AxCA-F-stathmin) by the COS-TPC method following the manufacturer's instructions. Adenoviruses containing cDNA of the longest isoform of human brain tau (AxCA-Tau4RWT), LacZ (AxCAi-LacZ), c-Jun N-terminal kinase (JNK) 3 (AxCA-JNK3), and Δ mitogen-activated protein kinase/extracellular signal-regulated kinase kinase kinase (MEKK) (AxCA-ΔMEKK) were also used [29]. COS-7 cells were maintained in Dulbecco's modified eagle's medium (DMEM) containing 10% fetal bovine serum (FBS) in a 5% CO_2/air chamber. For adenoviral expression, COS-7 cells were cultured in a six-well dish and exposed to recombinant viruses at various multiplicities of infection (MOI) in DMEM containing 5% FBS.

2.3. Cell fraction and Western blotting

COS-7 cells were gently washed with phosphate buffered saline 3 days after infection and lysed in Laemmli's sample buffer. Each of the fractions having equal start-cell counts were separated by 8% SDS–PAGE and electroblotted onto nylon membranes for immunoblot analyses as previously described [29]. MT-bound and -unbound tau were prepared as described previously [25]. Okadaic acid was added 1 day after infection of AxCA-Tau4RWT, and cells were lysed 24 h after treatment.

2.4. Immunocytochemistry

Cells were fixed with 4% paraformaldehyde for 10 min and permeabilized by 0.5% Triton X-100, followed by incubation with primary antibodies. Bound antibodies were visualized with Alexa dye-conjugated secondary antibodies (Molecular Probes) and observed with a confocal laser scanning microscope (Radiance 2000 KR3; Bio-Rad).

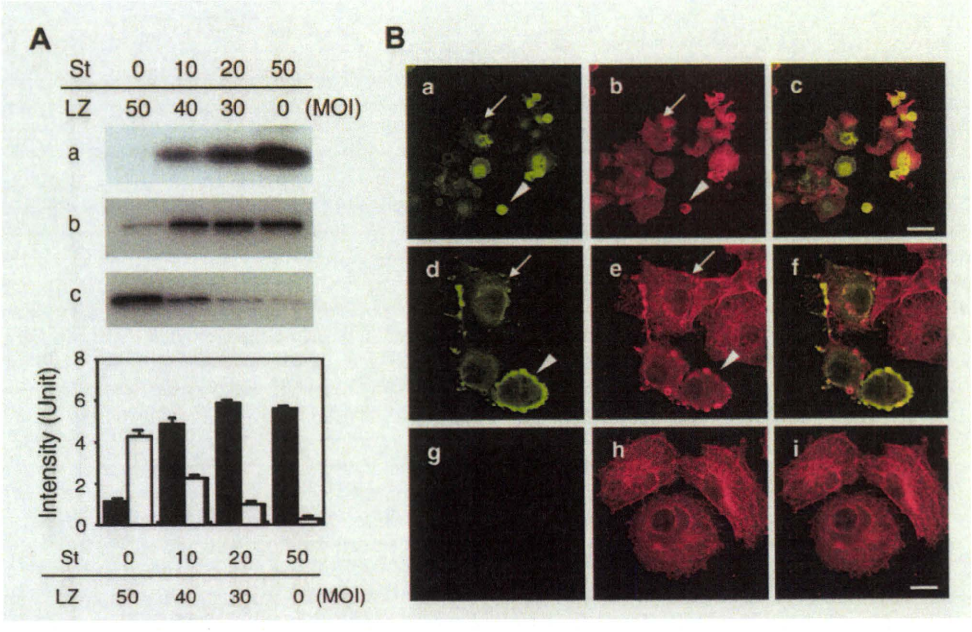

Fig. 1. Adenoviral induction of stathmin induces MT catastrophe in COS-7 cells. MT stability of COS-7 cells infected with AxCA-F-stathmin was analyzed by biochemical and immunocytochemical procedures. (A) Three days after infection with AxCA-F-stathmin (St) or AxCAi-LacZ (LZ) cDNA at the indicated MOI, the total amount of stathmin was evaluated by STC1 (a). Free (b) and polymerized tubulin (c) were fractioned as described in Section 2 and quantified by Western blotting using the anti-α-tubulin antibody, DM1A. The lower panel shows quantitative analyses of free (closed) or polymerized (open) tubulin in COS-7 cells. Each data point represents the means and standard error (S.E.) for three independent experiments. (B) 50 MOI of AxCA-F-stathmin-infected COS-7 cells (a–f) were co-labeled with STC1 (green) and DM1A (red), and observed by confocal laser scanning microscopy. It should be noted that the low level of stathmin expression induced mild MT disruption (arrow); however, high levels of stathmin expression caused cell to shrink (arrowhead). These abnormal cells were not observed in AxCAi-LacZ-infected cells (g–i). Merged images are shown in c, f, and i. Scale bars: a–c, 100 μm; d–i, 25 μm.

3. Results

3.1. Overexpression of stathmin induces MT catastrophe in COS-7 cell

In native neuronal cells, >90% of tau is bound to MTs [31]. However, excess exogenous tau generated by conventional transfection is not bound to MT (data not shown). To maintain the tau expression at relatively low levels and avoid undesired liberation of tau from MTs, we used an adenoviral-mediated transfection system in which about 80% of the expressed tau was held on MTs at five MOI of AxCA-Tau4RWT (data not shown).

The stathmin family is expressed in a wide variety of cells, including neurons. It binds to the ends of tubulin protofilament and induces MT catastrophe and/or tubulin sequestration [32–35]. In this study, we used stathmin to induce MT disruption in cells, and evaluated the effect of MT destruction on tau phosphorylation under physiological conditions. We first examined the effects of stathmin on MT structure in COS-7 cells. Three days after infection with AxCA-F-stathmin, FLAG-tagged stathmin expressed in an MOI-dependent manner (Fig. 1A, a). Along with increasing stathmin expression, the amount of polymerized tubulin decreased and that of soluble-free tubulin increased (Fig. 1A, b and c). The fraction of polymerized tubulin was greatly reduced in the cells infected with 50 MOI of AxCA-F-stathmin (Fig. 1A). To morphologically investigate MT catastrophe, COS-7 cells infected with 50 MOI of AxCAi-LacZ or AxCA-F-stathmin were double-labeled with

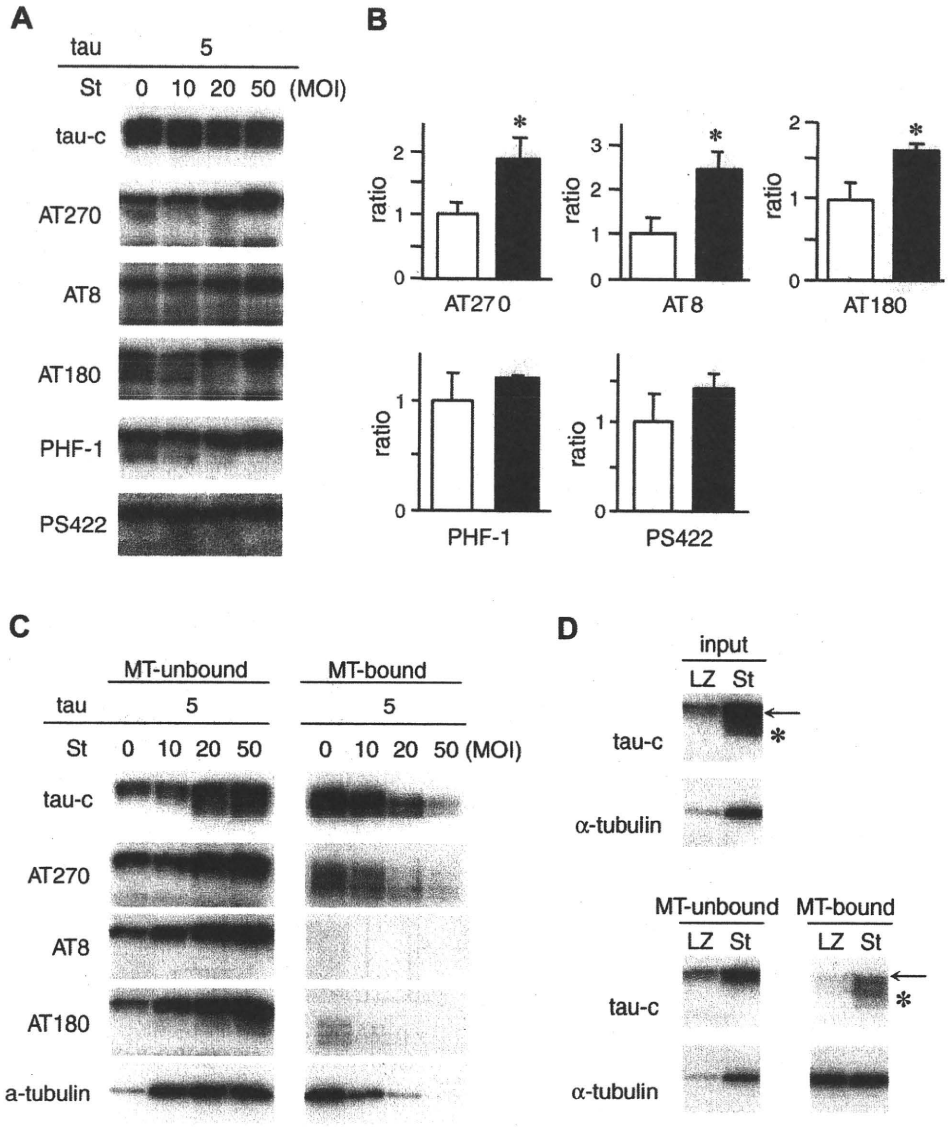

Fig. 2. Selective phosphorylation of tau induced by stathmin expression in MT-unbound fractions. COS-7 cells were co-infected with AxCA-Tau4RWT and AxCA-F-stathmin and the extent of tau phosphorylation was estimated by Western blotting using site-specific anti-phosphotau antibodies. (A) Total cell lysates from AxCA-Tau4RWT- and AxCA-F-stathmin-infected cells at the indicated MOI were separated by SDS–PAGE, and total (tau-c) and phosphorylated tau (AT270, AT8, AT180, PHF1, and PS422) were labeled by immunoblotting. (B) Quantitative analyses of tau phosphorylation in cells with (closed) or without (open) 50 MOI of AxCA-F-stathmin infection are shown. The intensities of the bands labeled with the indicated antibodies were normalized to those of total tau (tau-c). Data represent the means ± S.E. for three independent experiments. Statistical significance was evaluated using a Student's *t*-test (*$P < 0.05$). (C) MT-unbound and MT-bound fractions from AxCA-Tau4RWT and AxCA-F-stathmin-infected cells were subjected to Western blotting with the indicated antibodies. (D) MT-free tau from AxCAi-LacZ (LZ)- or AxCA-F-stathmin (St) infected cells (input) was remixed with cell lysate from naïve COS-7 cells, and fractioned according to MT binding. Each fraction was subjected to Western blotting using tau-c and DM1A (α-tubulin). The arrows and asterisks indicate slow migrating and faster migrating tau species, respectively.

anti-α-tubulin and anti-FLAG antibodies (Fig. 1B). Although the expression levels were slightly variable among cells, about 90% of the cells were labeled by the anti-FLAG antibody (data not shown). Moderate levels of stathmin expression resulted in decreased α-tubulin staining in COS-7 cells compared to naïve cells (Fig. 1B, d–f). High stathmin expression induced irregularly shrunken-shaped cells and destroyed MT structures in the cells (Fig. 1B, a–f). This was not observed in AxCAi-LacZ-infected cells (Fig. 1B, g–i).

3.2. Co-expression of stathmin enhances phosphorylation of tau associated with MT destruction

To examine the effects of stathmin on tau phosphorylation, COS-7 cells were co-infected with AxCA-Tau4RWT plus AxCAi-LacZ or AxCA-F-stathmin at different MOI, and the total cell lysates obtained were subjected to Western blotting using various anti-tau antibodies (Fig. 2A). Although the total amount of tau was not altered, the extent of phosphorylation of tau labeled by AT270 (Thr-181), AT8 (Ser-202 and Thr-205), and AT180 (Thr-231) increased along with increasing expression of stathmin in a MOI-dependent manner. There was statistical significance in the extent of tau phosphorylation between 0 and 50 MOI of AxCA-F-stathmin (Fig. 2B). The immunoreactivities with PHF-1 (phospho-Ser396 and -Ser404) and PS422 (phospho-Ser422) tended to slightly (but not significantly) increase. Thus, stathmin expression induced a higher extent of tau phosphorylation.

The ability of the MT-binding of tau in cells can be estimated by the fraction of the lysates under the presence of taxol [25]. In this procedure, MT-bound tau is co-fractioned into a pellet with taxol-stabilized MT, but MT-unbound tau is recovered in the supernatant. The total lysates from tau- and stathmin-expressing COS-7 cells were further fractioned by MT binding, and the phosphorylation of tau was analyzed by Western blotting. Along with MT disruption, the amount of MT-unbound tau increased. As seen in Fig. 2C, the MT-unbound tau migrated more slowly than MT-bound tau, indicating a higher phosphorylation of MT-unbound tau. This result was further confirmed by Western blotting using anti-phospho-tau antibodies, which showed that the phosphorylated tau occurred predominantly in the MT-unbound fraction (Fig. 2C).

One possible explanation for the predominance of tau in the MT-unbound fraction would be that the stathmin causes tau to liberate from MT via accelerating tau phosphorylation and reducing its affinity to MT. To determine whether tau was phosphorylated after being liberated from MTs, MT-unbound fractions from cells expressing AxCA-Tau4RWT plus AxCAi-LacZ or AxCA-F-stathmin (input in Fig. 2D) were remixed with cell homogenates from naïve COS-7 cells and subjected to the MT binding assay (Fig. 2D). If the tau in the MT-unbound fraction from stathmin-expressing cells were phosphorylated after being liberated from MTs, there would still have been some less phosphorylated tau, which can bind on taxol-stabilized MTs. Western blotting of total tau in the MT-unbound fraction from stathmin-expressing cells showed that soluble tau largely consisted of slow-migrating species and additional fast-migrating one. This finding suggested that a fraction of soluble tau contains relatively less phosphorylated tau species. Predictably, the slower migrating species did not bind to MTs, but the faster migrating tau species were still able to bind to MTs (Fig. 2D). The presence of tau having an MT-binding capacity in the MT-unbound fraction suggests that the tau was phosphorylated after being liberated from MT. Thus, stathmin expression induces tau liberation and its subsequent phosphorylation in parallel with MT disruption.

3.3. Stathmin expression induces activation of JNK

To examine whether certain protein kinases were activated by stathmin, total lysates from infected cells were subjected to Western blotting using antibodies that distinguish activated and inactivated forms of protein kinase (Fig. 3). Among the kinases

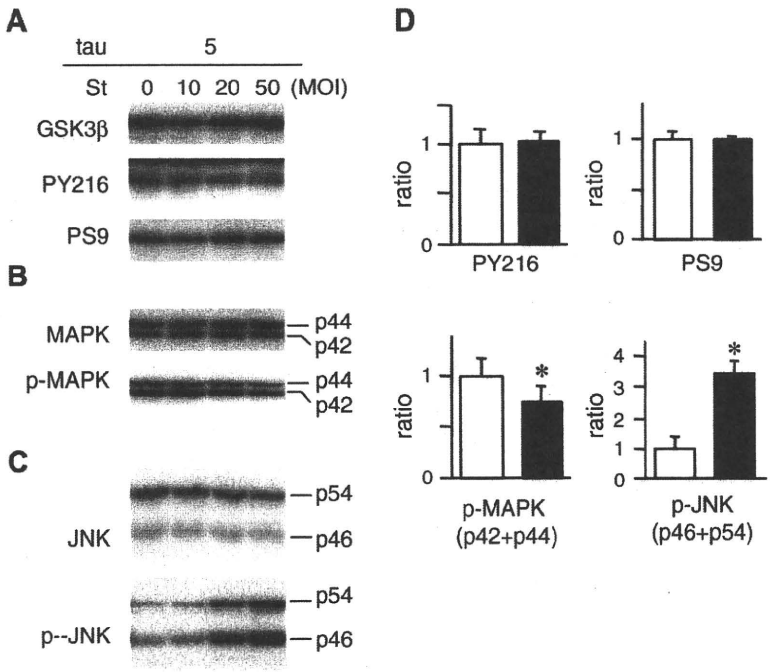

Fig. 3. Activation of JNK in stathmin-expressing cells. Effects of stathmin expression on the activity of GSK3β (A), MAPK (B), and JNK (C) were verified by Western blotting using specific antibodies labeled for the activated or inactivated form of each kinase. Total lysates were prepared from COS-7 cells co-infected with AxCA-Tau4RWT and AxCA-F-stathmin at the indicated MOI, and subjected to Western blotting using antibodies for total GSK3, phospho-Tyr216 (PY216), phospho-Ser9 (PS9), total MAPK (p42/p44), phospho-Thr202/Tyr204 (p-MAPK), total JNK (p46/p54), and phospho-Thr183/Tyr185 (p-JNK). (D) Quantitative analyses of fold kinase activation in cells with (closed) or without (open) 50 MOI of AxCA-F-stathmin infection are shown. Data represent the means ± S.E. for three independent experiments. Statistical significance was evaluated using a Student's *t*-test (*$P < 0.05$).

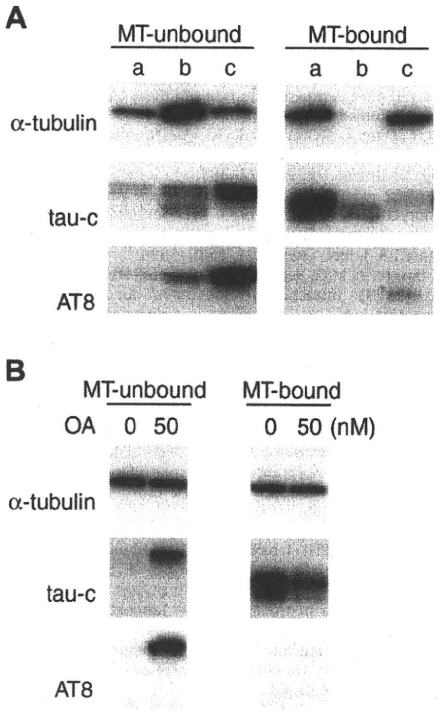

Fig. 4. Overexpression of JNK or inhibition of phosphatases induces tau phosphorylation but not MT disruption. (A) MT-unbound and -bound fractions from COS-7 cells co-infected with five MOI of AxCA-Tau4RWT and AxCAi-LacZ (110 MOI; a), AxCA-Tau4RWT and AxCA-F-stathmin (50 MOI; b), or AxCA-Tau4RWT and AxCA-JNK3 plus ΔMEKK (10 + 100 MOI; c) were subjected to Western blotting using DM1A (anti-α-tubulin), tau-c, and AT8. (B) Tau-expressing COS-7 cells were treated with or without 50 nM of okadaic acid and subjected to an MT-binding assay combined with Western blotting.

examined, JNKs (SAPK + JNK) were significantly activated and MAPK was left inactivated in the cells of the AxCA-F-stathmin infection as compared to those of the AxCAi-LacZ infection. The activity of glycogen synthase kinase 3 beta (GSK3β) was not altered throughout the experiment.

3.4. Activation of kinases or phosphatase inhibition induces tau phosphorylation but not MT disruption

The above data led us to presume that stathmin induces MT disruption and tau phosphorylation via JNK activation. To test this assumption, MT binding assays were performed in COS-7 cells expressing JNK3 and its activator ΔMEKK. As previously reported, AxCA-JNK3 plus AxCA-ΔMEKK infection increased tau phosphorylation at the AT8 sites; however, MT catastrophe was not observed (Fig. 4A). This result indicates that the activation of JNK can only induce tau phosphorylation but not MT disruption, and raises the idea that tau phosphorylation and MT disruption may be dissociated.

The extent of tau phosphorylation is also negatively regulated by phosphatases [36–39]. To probe whether the phosphatase inhibition induces MT disruption via tau phosphorylation, tau-expressing cells were treated with okadaic acid, a protein phosphatase-1 and -2A inhibitor. Although a high dose (250 nM) of okadaic acid induced both tau phosphorylation and MT disruption (data not shown), 50 nM okadaic acid solely induced tau phosphorylation without MT disassembly (Fig. 4B). Thus, enhanced tau phosphorylation by phosphatase inhibition cannot induce MT disruption. Taken together, our data indicate that tau phosphorylation is not sufficient for MT disruption.

4. Discussion

To our knowledge, this is the first report to demonstrate that MT disruption can induce subsequent tau phosphorylation. The extent of phosphorylation in MT-unbound tau produced by stathmin expression is higher than those of MT-bound tau. Given that JNK is activated by stathmin expression, it is possible that tau proteins were phosphorylated by JNK after being liberated from MTs. However, tau phosphorylation selectively occurred in the MT-unbound fraction (Fig. 2C), suggesting that the phosphorylation state of tau is more likely dependent on whether the expressed tau is bound with MT and that MT-unbound tau is a preferential substrate for kinases. Given that the stoichiometry of tubulin relative to tau is far greater than in healthy neurons, the amount of MT-unbound tau would be negligible under physiological conditions [31]. However, under abnormal conditions, such as the aberrant overproduction of tau and decreased expression or denaturation of tubulin, MT-unbound tau might be generated and be immediately hyperphosphorylated.

The effects of drug-induced MT disruption on tau phosphorylation have been reported previously; however, the results were in conflict with the present study [25]. This discrepancy may depend on MT-breaking-agents used in the study. Stathmin can sequestrate tubulin dimer(s) after MT destruction, and soluble tubulin dimer(s) likely remain to be bound to stathmin [27]. Although the physiological significance of soluble tubulin dimer is not known, it is conceivable that the numerous cellular factors can interact with them. Formation of stable tubulin–stathmin complex may interfere the interaction between tubulin dimers and such molecules including kinases, phosphatases, and tau. This may be that the concentrations of tubulin dimers were reduced similarly as in the neurons affected by tauopathy. In contrast, a small compound like nocodazole may not affect the binding between soluble tubulin dimers and other factors, and induce an increment in the soluble tubulin dimers. In this way, the amount of soluble tubulin dimers available for interaction with other molecules would be critical for tau phosphorylation.

In contrast to MT destruction inducing tau phosphorylation, MT destruction was not induced by the activation of certain kinases or by phosphatase inactivation, both of which can increase tau phosphorylation. Similar findings have been reported in anesthetized mice [40]. Therefore, these results suggest that tau phosphorylation, which may lead to the liberation of tau from MTs, does not have a profound effect on the stabilization of MTs, although the long-term effects of tau phosphorylation on MTs are remain unknown. Our results are also supported by recent findings that no differences exist between wild type and pseudo-phosphorylated tau in transgenic animals [41,42]. Taken together, tau phosphorylation alone may not be sufficient to induce MTs destruction and subsequent neurodegeneration.

This view can be readily applied to the pathogenesis of tauopathy, because the MT structure always disappear in affected neurons in the brains of AD patients [19,22]. Most neurons remain throughout a human lifetime, and MT disruption that leads to MT loss and/or tubulin degeneration can accidentally occur in aged neurons [21,22,43]. Newly expressed tau, which cannot bind to MTs, is then phosphorylated and accumulate in the neuronal cell body. If such an abnormality would be sustained over a long period, the accumulated tau may form NFT, which accompanies complete MT disruption as seen in brains affected by tauopathy. In fact, MT loss has also been found in non-NFT-bearing neurons in the brains of AD patients [22], and phosphorylated tau may gradually accumulate in the neuronal cell body for months [44].

The mechanisms inducing MT disruption in aged neurons remain obscure. Tubulin is a very unstable protein and easily loses

its potency at 37 °C for GTP/GDP exchange without GTP and protein-stabilizing compounds that have multiple hydroxyl groups [45]. Thus, it is possible that a reduced tubulin turnover rate and/or the reduced expression of factors required for tubulin maintenance can decrease the amount of MTs or tubulin in normal aging neurons [46]. Dysregulation of stathmin families could be other possible causes of MT dysregulation in aged or diseased neurons [28,47]. Furthermore, amyloid deposition, which is the other pathological hallmark of AD, may also lead to MT destabilization [48], suggesting that MT loss may be an intermediate between amyloid beta deposition and NFT formation in AD.

Acknowledgements

The authors thank M. Murayama for technical assistance and Dr. Y. Ihara for helpful discussion and comments. This work was partially supported by the JSPS KAKENHI, Grant-in-Aid for Young Scientists (B).

References

[1] Mohri, H. (1968) Amino-acid composition of "Tubulin" constituting microtubules of sperm flagella. Nature 217, 1053–1054.

[2] Hiller, G. and Weber, K. (1978) Radioimmunoassay for tubulin: a quantitative comparison of the tubulin content of different established tissue culture cells and tissues. Cell 14, 795–804.

[3] Downing, K.H. and Nogales, E. (1998) Tubulin structure: insights into microtubule properties and functions. Curr. Opin. Struct. Biol. 8, 785–791.

[4] Ikegami, K. and Setou, M. (2010) Unique post-translational modifications in specialized microtubule architecture. Cell Struct. Funct. 10, 20–30.

[5] Kirschner, M.W. and Mitchison, T. (1986) Microtubule dynamics. Nature 324, 621.

[6] van der Vaart, B., Akhmanova, A. and Straube, A. (2009) Regulation of microtubule dynamic instability. Biochem. Soc. Trans. 37, 1007–1013.

[7] Calligaris, D., Verdier-Pinard, P., Devred, F., Villard, C., Braguer, D. and Lafitte, D. (2010) Microtubule targeting agents: from biophysics to proteomics. Cell. Mol. Life Sci. 67, 1089–1104.

[8] Desai, A. and Mitchison, T.J. (1997) Microtubule polymerization dynamics. Annu. Rev. Cell Dev. Biol. 13, 83–117.

[9] Bommel, H., Xie, G., Rossoll, W., Wiese, S., Jablonka, S., Boehm, T. and Sendtner, M. (2002) Missense mutation in the tubulin-specific chaperone E (Tbce) gene in the mouse mutant progressive motor neuronopathy, a model of human motoneuron disease. J. Cell Biol. 159, 563–569.

[10] Martin, N., Jaubert, J., Gounon, P., Salido, E., Haase, G., Szatanik, M. and Guenet, J.L. (2002) A missense mutation in Tbce causes progressive motor neuronopathy in mice. Nat. Genet. 32, 443–447.

[11] Keays, D.A. (2007) Neuronal migration: unraveling the molecular pathway with humans, mice, and a fungus. Mamm. Genome 18, 425–430.

[12] Lindwall, G. and Cole, R.D. (1984) Phosphorylation affects the ability of tau protein to promote microtubule assembly. J. Biol. Chem. 259, 5301–5305.

[13] Yoshida, H. and Ihara, Y. (1993) Tau in paired helical filaments is functionally distinct from fetal tau: assembly incompetence of paired helical filament-tau. J. Neurochem. 61, 1183–1186.

[14] Hanger, D.P., Anderton, B.H. and Noble, W. (2009) Tau phosphorylation: the therapeutic challenge for neurodegenerative disease. Trends Mol. Med. 15, 112–119.

[15] Biernat, J. and Mandelkow, E.M. (1999) The development of cell processes induced by tau protein requires phosphorylation of serine 262 and 356 in the repeat domain and is inhibited by phosphorylation in the proline-rich domains. Mol. Biol. Cell 10, 727–740.

[16] Gomez-Isla, T., Hollister, R., West, H., Mui, S., Growdon, J.H., Petersen, R.C., Parisi, J.E. and Hyman, B.T. (1997) Neuronal loss correlates with but exceeds neurofibrillary tangles in Alzheimer's disease. Ann. Neurol. 41, 17–24.

[17] Grundke-Iqbal, I., Iqbal, K., Tung, Y.C., Quinlan, M., Wisniewski, H.M. and Binder, L.I. (1986) Abnormal phosphorylation of the microtubule-associated protein tau (tau) in Alzheimer cytoskeletal pathology. Proc. Natl. Acad. Sci. USA 83, 4913–4917.

[18] Ihara, Y., Nukina, N., Miura, R. and Ogawara, M. (1986) Phosphorylated tau protein is integrated into paired helical filaments in Alzheimer's disease. J. Biochem. 99, 1807–1810.

[19] Wood, J.G., Mirra, S.S., Pollock, N.J. and Binder, L.I. (1986) Neurofibrillary tangles of Alzheimer disease share antigenic determinants with the axonal microtubule-associated protein tau (tau). Proc. Natl. Acad. Sci. USA 83, 4040–4043.

[20] Gray, E.G., Paula-Barbosa, M. and Roher, A. (1987) Alzheimer's disease: paired helical filaments and cytomembranes. Neuropathol. Appl. Neurobiol. 13, 91–110.

[21] Paula-Barbosa, M., Tavares, M.A. and Cadete-Leite, A. (1987) A quantitative study of frontal cortex dendritic microtubules in patients with Alzheimer's disease. Brain Res. 417, 139–142.

[22] Cash, A.D. et al. (2003) Microtubule reduction in Alzheimer's disease and aging is independent of tau filament formation. Am. J. Pathol. 162, 1623–1627.

[23] Tatebayashi, Y. et al. (2002) Tau filament formation and associative memory deficit in aged mice expressing mutant (R406W) human tau. Proc. Natl. Acad. Sci. USA 99, 13896–13901.

[24] Miyasaka, T., Ding, Z., Gengyo-Ando, K., Oue, M., Yamaguchi, H., Mitani, S. and Ihara, Y. (2005) Progressive neurodegeneration in *C. elegans* model of tauopathy. Neurobiol. Dis. 20, 372–383.

[25] Merrick, S.E., Demoise, D.C. and Lee, V.M. (1996) Site-specific dephosphorylation of tau protein at Ser202/Thr205 in response to microtubule depolymerization in cultured human neurons involves protein phosphatase 2A. J. Biol. Chem. 271, 5589–5594.

[26] Sobel, A., Boutterin, M.C., Beretta, L., Chneiweiss, H., Doye, V. and Peyro-Saint-Paul, H. (1989) Intracellular substrates for extracellular signaling. Characterization of a ubiquitous, neuron-enriched phosphoprotein (stathmin). J. Biol. Chem. 264, 3765–3772.

[27] Curmi, P.A. et al. (1999) Stathmin and its phosphoprotein family: general properties, biochemical and functional interaction with tubulin. Cell Struct. Funct. 24, 345–357.

[28] Okazaki, T., Wang, H., Masliah, E., Cao, M., Johnson, S.A., Sundsmo, M., Saitoh, T. and Mori, N. (1995) SCG10, a neuron-specific growth-associated protein in Alzheimer's disease. Neurobiol. Aging 16, 883–894.

[29] Sato, S. et al. (2002) Aberrant tau phosphorylation by glycogen synthase kinase-3beta and JNK3 induces oligomeric tau fibrils in COS-7 cells. J. Biol. Chem. 277, 42060–42065.

[30] Otvos Jr., L., Feiner, L., Lang, E., Szendrei, G.I., Goedert, M. and Lee, V.M. (1994) Monoclonal antibody PHF-1 recognizes tau protein phosphorylated at serine residues 396 and 404. J. Neurosci. Res. 39, 669–673.

[31] Zhang, B. et al. (2004) Retarded axonal transport of R406W mutant tau in transgenic mice with a neurodegenerative tauopathy. J. Neurosci. 24, 4657–4667.

[32] Belmont, L.D. and Mitchison, T.J. (1996) Identification of a protein that interacts with tubulin dimers and increases the catastrophe rate of microtubules. Cell 84, 623–631.

[33] Jourdain, L., Curmi, P., Sobel, A., Pantaloni, D. and Carlier, M.F. (1997) Stathmin: a tubulin-sequestering protein which forms a ternary T2S complex with two tubulin molecules. Biochemistry 36, 10817–10821.

[34] Gigant, B. et al. (2000) The 4 A X-ray structure of a tubulin:stathmin-like domain complex. Cell 102, 809–816.

[35] Ravelli, R.B., Gigant, B., Curmi, P.A., Jourdain, I., Lachkar, S., Sobel, A. and Knossow, M. (2004) Insight into tubulin regulation from a complex with colchicine and a stathmin-like domain. Nature 428, 198–202.

[36] Gong, C.X., Shaikh, S., Wang, J.Z., Zaidi, T., Grundke-Iqbal, I. and Iqbal, K. (1995) Phosphatase activity toward abnormally phosphorylated tau: decrease in Alzheimer disease brain. J. Neurochem. 65, 732–738.

[37] Gong, C.X., Lidsky, T., Wegiel, J., Zuck, L., Grundke-Iqbal, I. and Iqbal, K. (2000) Phosphorylation of microtubule-associated protein tau is regulated by protein phosphatase 2A in mammalian brain. Implications for neurofibrillary degeneration in Alzheimer's disease. J. Biol. Chem. 275, 5535–5544.

[38] Pei, J.J., Gong, C.X., An, W.L., Winblad, B., Cowburn, R.F., Grundke-Iqbal, I. and Iqbal, K. (2003) Okadaic-acid-induced inhibition of protein phosphatase 2A produces activation of mitogen-activated protein kinases ERK1/2, MEK1/2, and p70 S6, similar to that in Alzheimer's disease. Am. J. Pathol. 163, 845–858.

[39] Liu, F., Grundke-Iqbal, I., Iqbal, K. and Gong, C.X. (2005) Contributions of protein phosphatases PP1, PP2A, PP2B and PP5 to the regulation of tau phosphorylation. Eur. J. Neurosci. 22, 1942–1950.

[40] Planel, E. et al. (2008) Anesthesia-induced hyperphosphorylation detaches 3-repeat tau from microtubules without affecting their stability in vivo. J. Neurosci. 28, 12798–12807.

[41] Brandt, R., Gergou, A., Wacker, I., Fath, T. and Hutter, H. (2009) A *Caenorhabditis elegans* model of tau hyperphosphorylation: induction of developmental defects by transgenic overexpression of Alzheimer's disease-like modified tau. Neurobiol. Aging 30, 22–33.

[42] Hundelt, M. et al. (2009) Altered phosphorylation but no neurodegeneration in a mouse model of tau hyperphosphorylation. Neurobiol. Aging.

[43] Borthwick, N.M., Yates, C.M. and Gordon, A. (1985) Reduced proteins in temporal cortex in Alzheimer's disease: an electrophoretic study. J. Neurochem. 44, 1436–1441.

[44] Miyasaka, T. et al. (2005) Visualization of newly deposited tau in neurofibrillary tangles and neuropil threads. J. Neuropathol. Exp. Neurol. 64, 665–674.

[45] Arai, T., Ihara, Y., Arai, K. and Kaziro, Y. (1975) Purification of tubulin from bovine brain and its interaction with guanine nucleotides. J. Biochem. 77, 647–658.

[46] Fanara, P. et al. (2007) Stabilization of hyperdynamic microtubules is neuroprotective in amyotrophic lateral sclerosis. J. Biol. Chem. 282, 23465–23472.

[47] Mori, N. and Morii, H. (2002) SCG10-related neuronal growth-associated proteins in neural development, plasticity, degeneration, and aging. J. Neurosci. Res. 70, 264–273.

[48] King, M.E., Kan, H.M., Baas, P.W., Erisir, A., Glabe, C.G. and Bloom, G.S. (2006) Tau-dependent microtubule disassembly initiated by prefibrillar beta-amyloid. J. Cell Biol. 175, 541–546.

Circulation Research
JOURNAL OF THE AMERICAN HEART ASSOCIATION

American Heart Association®
Learn and Live℠

Promotion of CHIP-Mediated p53 Degradation Protects the Heart From Ischemic Injury

Atsuhiko T. Naito, Sho Okada, Tohru Minamino, Koji Iwanaga, Mei-Lan Liu, Tomokazu Sumida, Seitaro Nomura, Naruhiko Sahara, Tatsuya Mizoroki, Akihiko Takashima, Hiroshi Akazawa, Toshio Nagai, Ichiro Shiojima and Issei Komuro

Circ. Res. 2010;106;1692-1702; originally published online Apr 22, 2010;
DOI: 10.1161/CIRCRESAHA.109.214346
Circulation Research is published by the American Heart Association. 7272 Greenville Avenue, Dallas, TX 72514
 Print ISSN: 0009-7330. Online ISSN: 1524-4571

Promotion of CHIP-Mediated p53 Degradation Protects the Heart From Ischemic Injury

Atsuhiko T. Naito, Sho Okada, Tohru Minamino, Koji Iwanaga, Mei-Lan Liu, Tomokazu Sumida, Seitaro Nomura, Naruhiko Sahara, Tatsuya Mizoroki, Akihiko Takashima, Hiroshi Akazawa, Toshio Nagai, Ichiro Shiojima, Issei Komuro

Rationale: The number of patients with coronary heart disease, including myocardial infarction, is increasing and novel therapeutic strategy is awaited. Tumor suppressor protein p53 accumulates in the myocardium after myocardial infarction, causes apoptosis of cardiomyocytes, and plays an important role in the progression into heart failure.

Objectives: We investigated the molecular mechanisms of p53 accumulation in the heart after myocardial infarction and tested whether anti-p53 approach would be effective against myocardial infarction.

Methods and Results: Through expression screening, we found that CHIP (carboxyl terminus of Hsp70-interacting protein) is an endogenous p53 antagonist in the heart. CHIP suppressed p53 level by ubiquitinating and inducing proteasomal degradation. CHIP transcription was downregulated after hypoxic stress and restoration of CHIP protein level prevented p53 accumulation after hypoxic stress. CHIP overexpression in vivo prevented p53 accumulation and cardiomyocyte apoptosis after myocardial infarction. Promotion of CHIP function by heat shock protein (Hsp)90 inhibitor, 17-allylamino-17-demethoxy geldanamycin (17-AAG), also prevented p53 accumulation and cardiomyocyte apoptosis both in vitro and in vivo. CHIP-mediated p53 degradation was at least one of the cardioprotective effects of 17-AAG.

Conclusions: We found that downregulation of CHIP level by hypoxia was responsible for p53 accumulation in the heart after myocardial infarction. Decreasing the amount of p53 prevented myocardial apoptosis and ameliorated ventricular remodeling after myocardial infarction. We conclude that anti-p53 approach would be effective to treat myocardial infarction. (*Circ Res*. 2010;106:1692-1702.)

Key Words: myocardial infarction ■ CHIP ■ p53 ■ hypoxia

The number of patients with coronary heart disease has been increasing and cardiovascular diseases are the leading cause of deaths in the Western world. Despite the development of pharmacological and nonpharmacological interventions, 33% of the men and 43% of the women die within 5 years after myocardial infarction (MI).[1] Therefore, a novel therapeutic approach against coronary heart disease is awaited.

Apoptosis of cardiomyocytes is accompanied with acute coronary occlusion.[2] Because apoptotic loss of cardiomyocytes causes heart failure,[3] inhibition of apoptosis has been suggested as an additional therapeutic approach to coronary heart disease.[4] In mice, overexpression of antiapoptotic Bcl-2 protein or genetic deletion of proapoptotic Bax protein have been reported to prevent apoptosis and reduce infarct size,[5–8] implicating that antiapoptotic approach is effective for prevention of ventricular remodeling after myocardial infarction.

The tumor suppressor *p53* is an important transcription factor that regulates cell cycle progression, cellular senescence, and apoptosis. Under physiological condition, p53 protein level is maintained low, but is elevated when cells are stressed or damaged.[9] The mechanism for keeping p53 protein level low involves several E3 ubiquitin ligases such as MDM2,[10,11] COP1,[12] and Pirh2.[13] Importantly, the expression of these proteins were positively regulated by p53, suggesting the role for negative-feedback loop against p53 elevation.

Protein level of p53 is also kept low in the heart but it is elevated when cardiac cells are exposed to hypoxia.[14–16]

Original received December 4, 2009; revision received April 6, 2010; accepted April 12, 2010.

From the Department of Cardiovascular Science and Medicine (A.T.N., S.O., T. Minamino, K.I., M.-L.L., T.S., S.N., H.A., T.N., I.S., I.K.), Chiba University Graduate School of Medicine, Japan; Department of Cardiovascular Medicine (A.T.N., H.A., I.S., I.K.), Osaka University Graduate School of Medicine, Japan; PRESTO (T. Minamino), Japan Science and Technology Agency, Saitama, Japan; and Laboratory for Alzheimer's Disease (N.S., T. Mizoroki, A.T.). RIKEN Brain Science Institute, Saitama, Japan.

This manuscript was sent to Junichi Sadoshima, Consulting Editor, for review by expert referees, editorial decision, and final disposition.

Correspondence to Issei Komuro, MD, PhD, Department of Cardiovascular Science and Medicine, Chiba University Graduate School of Medicine, 1-8-1 Inohana, Chuo-ku, Chiba, Japan. E-mail komuro-tky@umin.ac.jp

Circulation Research **is available at http://circres.ahajournals.org** **DOI: 10.1161/CIRCRESAHA.109.214346**

We have recently reported that elevation of p53 causes the development of pressure overload-induced heart failure.[16] We have also observed the elevation of p53 protein levels after myocardial infarction and shown that *p53* gene deletion improved cardiac function after myocardial infarction,[16] suggesting that the inhibition of p53 might become a novel therapeutic strategy for ischemic heart diseases.

As an initial approach for the investigation of anti-p53 therapy, we searched for an endogenous p53 antagonist in the heart. Through expression screening, we found that CHIP (carboxyl terminus of Hsp70-interacting protein) is an endogenous p53 antagonist that keeps p53 level low in the heart. We also found that CHIP downregulation is involved in the mechanism of p53 accumulation in the heart after myocardial infarction. Facilitating CHIP-mediated p53 degradation prevented apoptosis of cardiomyocytes and ameliorated ventricular remodeling in the postinfarct heart. The present study revealed the mechanism of p53 accumulation in the heart after myocardial ischemia and suggested that anti-p53 approach would be effective to treat myocardial infarction.

Non-standard Abbreviations and Acronyms

17-AAG	17-allylamino-17-demethoxy geldanamycin
CHIP	carboxyl terminus of Hsp70-interacting protein
HIF	hypoxia-inducible factor
HRE	hypoxia-responsive element
Hsp	heat shock protein
HW/BW	heart weight/body weight
MI	myocardial infarction
PARP	poly(ADP-ribose)polymerase
siRNA	small interfering RNA

Methods

Expression Cloning

Expression cloning was performed as described previously[17] using PG13-Luc (kind gift from B. Vogelstein, Ludwig Center for Cancer Genetics and Therapeutics, Howard Hughes Medical Institute, and Sidney Kimmel Cancer Center, Johns Hopkins Medical Institutions, Baltimore, Md) as a reporter plasmid. Initially, cDNA expression library from human heart (Invitrogen) was separated into small pools that contain ≈100 clones each. cDNA clones that downregulate PG13 activity were isolated by sib-selection.

Cell Culture

COS7 and HEK293 cells are from ATCC and cultured in DMEM containing 10% FBS (Invitrogen). Neonatal rat cardiomyocytes were isolated from 1-day-old Wistar rats and cultured as described previously.[18] Cardiomyocytes were exposed to hypoxic stress by culturing under $CoCl_2$ or by culturing in hypoxic chamber (<1% O_2; Po_2, 18 to ≈20 mm Hg).

Animals

All protocols were approved by Chiba University review board. CHIP knockout mice and cardiac-specific inducible hypoxia-inducible factor (HIF)-1 knockout mice were described.[16,19,20] Heterozygous CHIP knockout mice were used in this study because homozygous knockout mice were perinatally lethal.[20] Cardiac-specific CHIP transgenic mice were generated by pronuclear injection of αMHC-HA-CHIP transgene construct. Coronary artery ligation was performed on 10-week old male mice as described previously.[21]

Statistical Analysis

Data are expressed as means±SE. The significance of differences among means was evaluated using analysis of variance (ANOVA), followed by Fisher's protected least significant difference test and Dunnett's test for multiple comparisons. Significant differences were defined as $P<0.05$.

Results

Identification of CHIP As a Novel p53 Antagonist From Heart cDNA Library

To elucidate novel p53 antagonists in the heart, we performed expression screening by expressing cDNA pools in COS7 cells together with a reporter plasmid, PG13-luciferase, which contains 13 copies of p53 binding site upstream of luciferase gene and responsive to wild-type p53 dependent transcription. From the screening of 500 cDNA pools, each containing around 100 individual cDNA clones obtained from human heart cDNA library, we found 5 pools that suppress the PG13 activity. Individual cDNA clone that downregulates the PG13 activity was identified by sib-selection. One of the molecules that was highly expressed in the heart (Figure I, A, in the Online Data Supplement, available at http://circres.ahajournals.org) was CHIP (also called STUB1 [Stip1 homology and U-box containing protein]), a chaperone-interacting protein with E3 ubiquitin ligase activity.[22] Transfection of CHIP suppressed endogenous and exogenous (by overexpression of p53) PG13 activity (Figure 1A) and decreased the protein levels of p53 (Figure 1B) in a plasmid dose-dependent manner in COS7 cells. Direct interaction between CHIP and p53 was confirmed both at the exogenous level in COS7 cells (Online Figure I, B) and at the endogenous level in cardiomyocytes (Online Figure I, C). Western blotting using anti-ubiquitin antibody after immunoprecipitation with p53 revealed that overexpression of CHIP increased poly-ubiquitinated p53 (which appears as a smear) (Online Figure I, D). The proteasomal inhibitor MG132 restored p53 protein level that was suppressed by CHIP (Online Figure I, E), indicating that CHIP directs p53 for proteasome-mediated degradation. When CHIP was knocked down in cardiomyocytes using small interfering (si)RNA, p53 expression was upregulated (Figure 1C), and p53 protein levels following CHIP knockdown were comparable to those induced by the knockdown of MDM2, a well known E3 ubiquitin ligase for p53 (Figure 1D). CHIP protein level was not changed by knockdown of MDM2 (Figure 1D). p53 protein levels were also markedly elevated in the heart of CHIP heterozygous mice (Figure 1E). These results suggest that CHIP induces degradation of wild-type p53 protein in cardiomyocytes, which is consistent with previous reports in other cells (H1299 cells and U2OS cells).[23,24] In addition, we revealed that CHIP is a crucial negative regulator that keeps p53 protein levels low in the heart under physiological conditions.

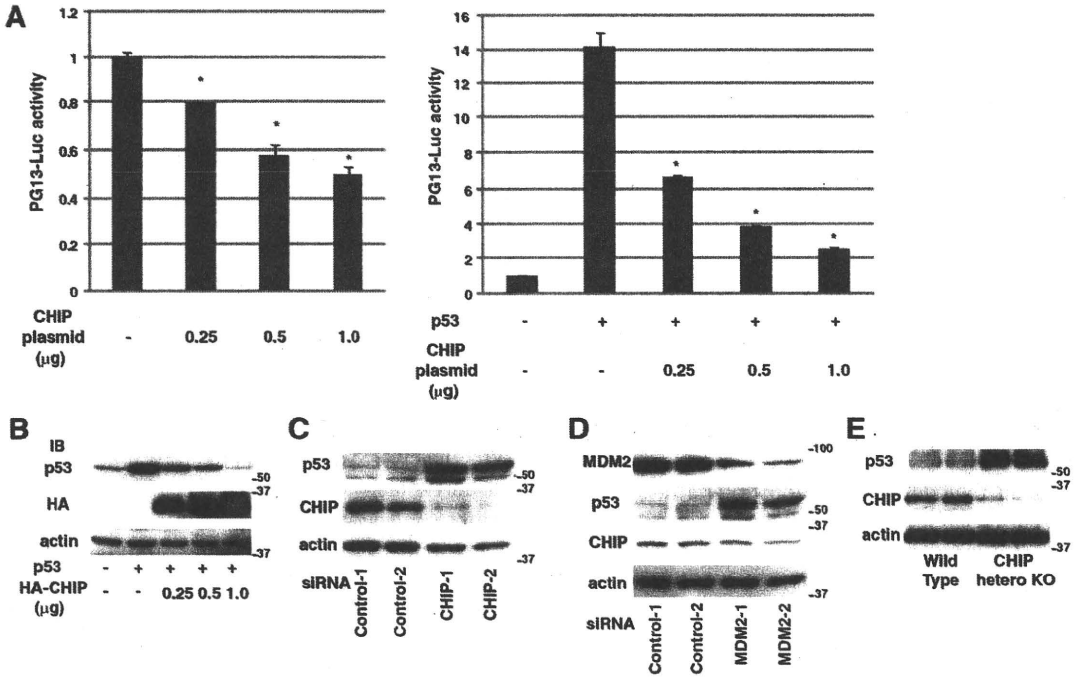

Figure 1. CHIP is a crucial negative regulator of p53 expression in the heart. A, Transfection of CHIP expressing plasmid suppressed endogenous **(left)** and exogenous **(right)** p53 transcriptional activity. *$P<0.01$ vs control; n=5. **B,** CHIP decreases p53 protein levels in COS7 cells. IB indicates immunoblot. **C,** p53 expression is upregulated by CHIP knockdown in cardiomyocytes. siRNAs specific to CHIP (CHIP-1 and CHIP-2), or control siRNA were transfected into cultured cardiomyocytes and protein levels of CHIP and p53 were examined by Western blotting. CHIP-1 and CHIP-2 represent 2 different siRNAs against CHIP. Control-1 is a commercially available control RNA, and control-2 is a scrambled control RNA. **D,** p53 upregulation is also observed by MDM2 knockdown. siRNAs specific to MDM2 (MDM2–1 and MDM2–2) or control siRNA were transfected into cultured cardiomyocytes, and protein levels of CHIP, p53, and MDM2 were examined by Western blotting. The extent of p53 upregulation by MDM2 knockdown was comparable to that induced by CHIP knockdown. **E,** Total protein of wild-type and CHIP heterozygous mice were analyzed by Western blotting. p53 expression is upregulated in the heart of CHIP heterozygous mice.

Molecular Mechanisms of Hypoxia-Induced p53 Accumulation

As CHIP regulates p53 status in the heart, we speculated that CHIP might be involved in the molecular mechanism of hypoxia-induced p53 accumulation in the heart. Cobalt chloride ($CoCl_2$) increases HIF-1 activity through preventing HIF-1α protein degradation and is widely used as a hypoxia mimicking reagent.[25,26] Treatment of cardiomyocytes with $CoCl_2$ (250 μmol/L) increased p53 protein level with a marked downregulation of CHIP protein level (Figure 2A). Notably, the expression of MDM2 was rather increased in this experimental condition. Because transcriptional regulation of MDM2 is known to be upregulated by p53 as a part of negative-feedback loop, increased MDM2 expression after $CoCl_2$ treatment may possibly be attributable to this feedback system against p53 elevation. Accumulation of p53 and downregulation of CHIP were also observed when cardiomyocytes were cultured in hypoxic chamber for 24 hours (Online Figure I, F). We confirmed that both treatments increased nuclear HIF-1α protein that binds to HIF-1α binding oligonucleotide by commercially available ELISA system (Online Figure I, G). We also analyzed the expression of p53 and CHIP in the heart after MI. p53 protein levels were increased on day 1 after MI and remained upregulated thereafter, whereas expression levels of CHIP were markedly downregulated on day 1, and remained at lower levels than those of controls (Figure 2B and analyzed in Online Figure II, A and B). In contrast, MDM2 protein levels were slightly increased after MI (Figure 2B). The inverse correlation between CHIP and p53 protein level implies the possible involvement of CHIP downregulation in the initiation of p53 accumulation after acute hypoxic stress. Other E3 ubiquitin ligases whose transcription is regulated by p53, such as MDM2, might work to reverse p53 level after initial accumulation of p53 as a feedback system to prevent further detrimental effects that might be elicited by chronic p53 elevation.

To investigate why CHIP is downregulated after hypoxic insult, we tested whether HIF-1 mediates hypoxia-induced downregulation of CHIP, because HIF-1 is known to downregulate some of its target genes through hypoxia-responsive element (HRE).[27–30] Human CHIP promoter (from −329 bases upstream of transcription start site to +39 bases downstream of transcription start site) that contains a conserved HRE at −49 (Figure 2C) was cloned upstream of luciferase reporter gene (pGL4-CHIP). pGL4-CHIP activity was significantly suppressed by both $CoCl_2$ treatment (24 hours) and HIF-1α overexpression in COS7 cells (Figure 2D). When a mutation was introduced into HRE at −49 (pGL4-CHIP-mutHRE), the luciferase activity was no longer responsive to hypoxic stress or HIF-1α overexpression (Figure 2D), suggesting that *CHIP* gene expression is downregu-

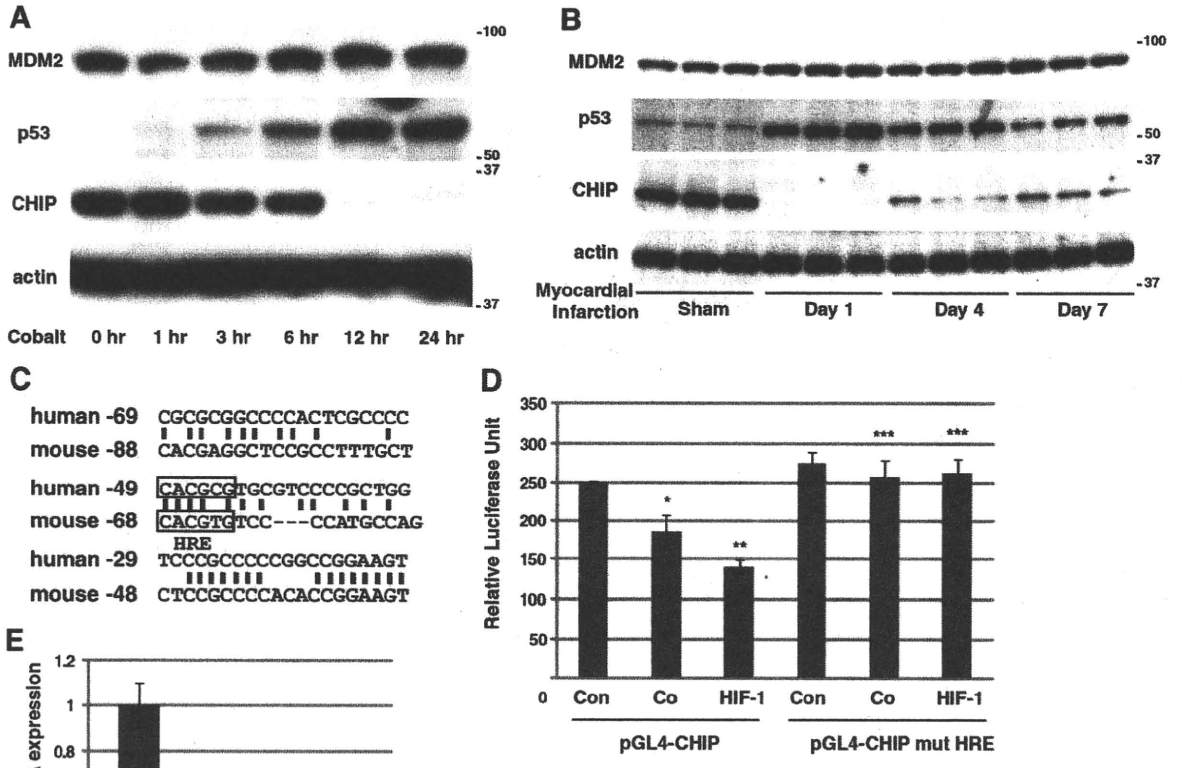

Figure 2. CHIP is downregulated by hypoxic stress. A, $CoCl_2$-induced p53 accumulation is associated with CHIP downregulation in cardiomyocytes. Cardiomyocytes were treated with 250 μmol/L $CoCl_2$, and protein was extracted at the indicated time point. **B,** Experimental myocardial infarction was created by permanent ligation of the coronary artery. Protein samples were extracted from total heart at the indicated time point after coronary artery ligation. CHIP expression is downregulated and p53 expression is upregulated after MI. **C,** Sequence comparison of human and mouse CHIP promoter. **Boxes** indicate conserved HRE. **D,** CHIP promoter activity is downregulated by $CoCl_2$ treatment and HIF-1α overexpression, and mutations (CACGTG to CTGGCG) introduced into HRE at −49 abrogated this response. CHIP promoter sequence from human genomic DNA (−329 to +39 from transcription start site) was cloned upstream of luciferase gene. Mutation was introduced using a kit from Stratagene. Luciferase assay was performed 24 hours after $CoCl_2$ treatment or HIF-1α overexpression. *$P<0.05$, **$P<0.01$, ***P=NS vs control; n=5. **E,** Real-time PCR analysis revealed mRNA level of CHIP was also downregulated by hypoxic stress (Co) and HIF-1α overexpression. RNA was extracted 24 hours after $CoCl_2$ treatment or HIF-1α overexpression. *$P<0.01$.

lated by HIF-1 at the transcriptional level through HRE. Real-time PCR analysis revealed that exposure of cardiomyocytes to $CoCl_2$ (24 hours) and adenoviral overexpression of constitutively active HIF-1α led to marked downregulation of CHIP mRNA levels (Figure 2E), further supporting our data that hypoxic stress downregulates CHIP levels. HIF-1α gene is both required and sufficient for hypoxic stress-induced CHIP downregulation and p53 accumulation because knockdown of HIF-1α attenuated the effects of $CoCl_2$ treatment on expressions of p53 and CHIP (Online Figure III, A), and overexpression of constitutively active HIF-1α suppressed CHIP expression and increased p53 expression in cardiomyocytes (Online Figure III, B). Furthermore, downregulation of CHIP protein levels after MI was attenuated in cardiac-specific inducible HIF-1α conditional knockout mice[16] (Online Figure III, C). Collectively, these findings suggest that CHIP transcription is directly downregulated by hypoxia through HIF-1.

CHIP Protects Cardiomyocytes From Hypoxia-Induced p53-Mediated Apoptosis of Cardiomyocytes

Because hypoxia or p53 overexpression induces apoptotic cell death in cultured cardiomyocytes,[14] we next examined whether hypoxia-induced cardiomyocyte apoptosis is mediated by the HIF-1-CHIP-p53 pathway. $CoCl_2$ treatment (24 hours) induced p53 accumulation and promoted apoptosis of cardiomyocytes as assessed by cleaved poly (ADP-ribose) polymerase (PARP) expression (Figure 3A), Annexin V staining (Figure 3B and 3C), and caspase-3 activity (Figure 3D). $CoCl_2$-induced apoptosis was p53-dependent, because knockdown of p53 in $CoCl_2$-treated cardiomyocytes attenuated hypoxia-induced cell death (Figure 3A through 3D). We next assessed whether overexpression of CHIP could rescue $CoCl_2$-induced apoptosis. Adenovirus-mediated overexpression of CHIP in cardiomyocytes markedly downregulated p53 expression and attenuated apoptosis in $CoCl_2$-treated

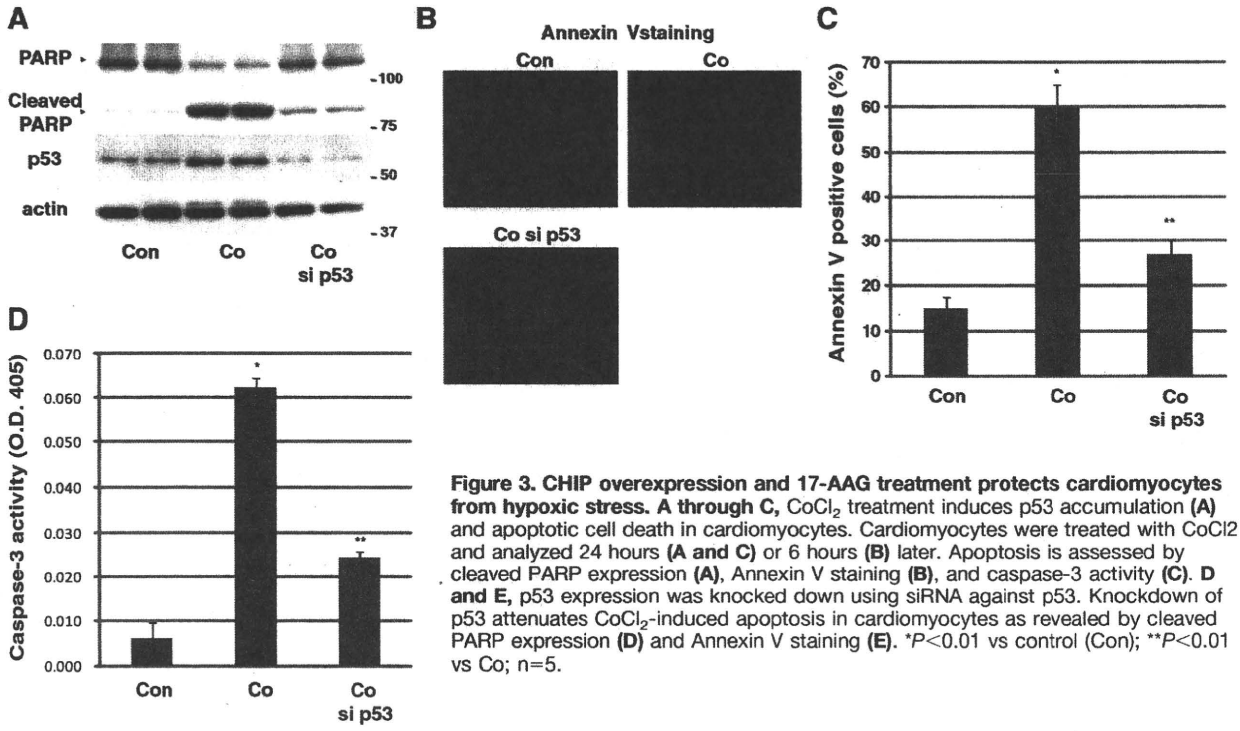

Figure 3. CHIP overexpression and 17-AAG treatment protects cardiomyocytes from hypoxic stress. A through C, $CoCl_2$ treatment induces p53 accumulation **(A)** and apoptotic cell death in cardiomyocytes. Cardiomyocytes were treated with CoCl2 and analyzed 24 hours **(A and C)** or 6 hours **(B)** later. Apoptosis is assessed by cleaved PARP expression **(A)**, Annexin V staining **(B)**, and caspase-3 activity **(C)**. **D and E,** p53 expression was knocked down using siRNA against p53. Knockdown of p53 attenuates $CoCl_2$-induced apoptosis in cardiomyocytes as revealed by cleaved PARP expression **(D)** and Annexin V staining **(E)**. *$P<0.01$ vs control (Con); **$P<0.01$ vs Co; n=5.

cardiomyocytes (Figure 4A through 4C). These results underscore our hypothesis that downregulation of CHIP is responsible for p53 accumulation after hypoxic stress. Moreover, forced expression of CHIP prevented hypoxia-induced cardiomyocyte apoptosis by inducing degradation of p53, suggesting that CHIP-mediated p53 degradation is a potential therapeutic target.

17-AAG Protects Cardiomyocytes From Hypoxia-Induced Apoptosis

Inhibitors for heat shock protein (Hsp)90 have been shown to promote proteasomal degradation of CHIP client proteins and to be effective for the diseases caused by the accumulation of CHIP substrates.[31,32] We therefore examined whether an Hsp90 inhibitor 17-allylamino-17-demethoxy geldanamycin (17-AAG) induces degradation of p53 protein and protects cardiomyocytes from hypoxic stress. In cardiomyocytes treated with $CoCl_2$, 17-AAG downregulated p53 expression (Figure 4D). 17-AAG treatment also suppressed hypoxia-induced cardiomyocyte apoptosis in a CHIP-dependent manner, because CHIP knockdown attenuated the protective effects of 17-AAG (Figure 4E through 4G). These results suggest that 17-AAG protects cardiomyocytes from hypoxic stress by promoting CHIP-mediated p53 degradation.

Interestingly, protein level of CHIP was increased by 17-AAG treatment (Figure 4E). As mRNA level of CHIP was not changed by 17-AAG treatment (Online Figure IV, A), we speculated that protein stability was affected by 17-AAG treatment. When protein translation was inhibited by cycloheximide, 17-AAG treatment dramatically extended the protein half-life of CHIP (Online Figure IV, B and C). 17-AAG also upregulated the protein stability of other proteins, Hsp70 and HSF-1 (Online Figure IV, B and C). Because 17-AAG exerted some antiapoptotic effects even in the cells of negligible CHIP protein level (Figure 4E and 4F), upregulation of these cardioprotective proteins[33,34] might mediate part of the effects of 17-AAG. It remains to be determined how 17-AAG prolongs protein half-life of certain kinds of proteins.

CHIP and 17-AAG Prevent Apoptosis and Ventricular Remodeling After Myocardial Infarction

We next examined whether promotion of CHIP-mediated p53 degradation could attenuate ischemic cardiac injury also in vivo. For this purpose, transgenic mice which overexpress CHIP specifically in the heart (CHIP-Tg) (Figure 5A) were subjected to permanent coronary artery ligation. In CHIP-Tg mice, elevation of p53 protein levels (Figure 5B) and apoptotic cardiomyocyte death in the border zone of the infarct area (Figure 5B and 5C) were attenuated compared to wild-type littermates at 24 hours after the MI operation. Apoptotic death of the cardiomyocytes in the remote zone of the infarct was not changed between littermates (data not shown). We next examined whether this decrease in apoptotic cell death leads to attenuation of cardiac ventricular remodeling. At day 14, CHIP-Tg mice exhibited smaller heart weight/body weight (HW/BW) ratio, better contractility and less ventricular remodeling (Figure 5D and 5E) compared to wild-type littermates. These results provides an evidence for our hypothesis that CHIP downregulation is responsible for p53 accumulation after myocardial infarction, and suggests that CHIP overexpression is protective for the heart by preventing p53 accumulation and cardiomyocyte apoptosis after myocardial infarction.

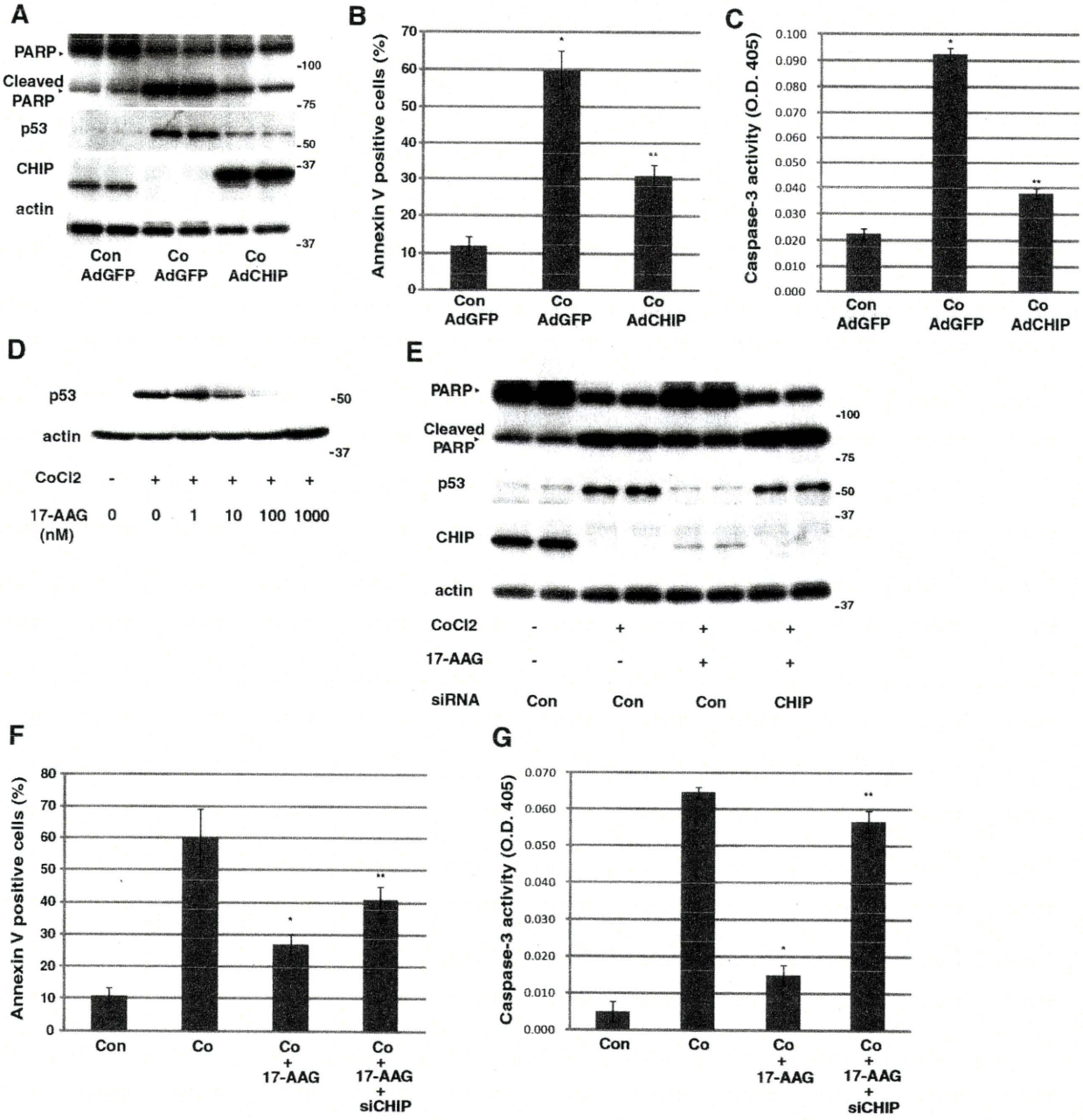

Figure 4. Promoting CHIP-mediated p53 degradation is protective against hypoxic stress. A through C, Overexpression of CHIP attenuates $CoCl_2$-induced p53 accumulation **(A)** and apoptosis in cardiomyocytes. Cardiomyocytes were infected with adenovirus harboring green fluorescent protein (GFP) or CHIP. Twenty-four hours later, culture medium was changed and the cells were treated with $CoCl_2$. Apoptosis was assessed by cleaved PARP expression **(A)**, Annexin V staining **(B)**, and caspase-3 activity **(C)**. $^*P<0.01$ vs control (Con)+AdGFP; $^{**}P<0.01$ vs Co+AdGFP; n=5. **D,** 17-AAG downregulates p53 expression in cardiomyocytes. Neonatal rat cardiomyocytes were treated with $CoCl_2$ with or without 17-AAG at the indicated concentration. **E through G,** 17-AAG inhibits $CoCl_2$-induced p53 accumulation **(E)** and apoptosis in cardiomyocytes, which is abrogated by CHIP knockdown. Neonatal rat cardiomyocytes were transfected with control siRNA or siRNA against CHIP. Twenty-four hours later, medium was changed and the cells were treated with $CoCl_2$ and/or 17-AAG. Apoptosis is assessed by cleaved PARP expression **(E)**, Annexin V staining **(F)**, and caspase-3 activity **(G)**. $^*P<0.01$ vs Co; $^{**}P<0.05$ vs Co +17-AAG; n=3.

We also examined whether treatment with 17-AAG exerts similar cardioprotective effects. 17-AAG (10 mg/kg) or vehicle was intraperitoneally injected immediately after permanent coronary artery ligation. This single injection of 17-AAG effectively suppressed the elevation of p53 protein levels and apoptotic cell death in the border zone of the infarct area at 24 hours after the operation (Figure 6A and 6B). As p53 protein level was kept elevated even 4 and 7 days after MI (Figure 2B), 17-AAG was injected every other days and we assessed whether 17-AAG treatment also leads to attenuation of ventricular remodeling, as observed in CHIP-Tg mice. At day 14, mice treated with 17-AAG exhibited smaller HW/BW ratio, better contractility,